Originally published as:

Fu, J., Jian, Y., Wang, X., Li, L., Ciais, P., Zscheischler, J., Wang, Y., Tang, Y., Müller, C., Webber, H., Yang, B., Wang, Q., Cui, X., Huang, W., Liu, Y., Zhao, P., Piao, S., Zhou, F. (2023): Extreme rainfall reduces one-twelfth of China's rice yield over the last two decades. - Nature Food, 4, 416-426.

DOI: https://doi.org/10.1038/s43016-023-00753-6

Extreme rainfall reduces one-twelfth of China's rice yield over the last two decades

Jin Fu[1]†, Yiwei Jian[1]†, Xuhui Wang[1]†, Laurent Li[2], Philippe Ciais[3,4], Jakob Zscheischler[5], Yin Wang[6], Yanhong Tang[6], Christoph Müller[7], Heidi Webber[8], Bo Yang[9], Yali Wu[10], Qihui Wang[1], Xiaoqing Cui[1], Weichen Huang[1], Yongqiang Liu[11], Pengjun Zhao[12], Shilong Piao[1], Feng Zhou[1]*

[1]Institute of Carbon Neutrality, Laboratory for Earth Surface Processes, College of Urban and Environmental Sciences, Peking University; Beijing, China.

[2]Laboratoire de Météorologie Dynamique, CNRS, Sorbonne Université; Paris, France.

[3]Laboratoire des Sciences du Climat et de l'Environnement, LSCE; Gif sur Yvette, France.

[4]Climate and Atmosphere Research Center (CARE-C), The Cyprus Institute; Nicosia, Cyprus.

[5]Department of Computational Hydrosystems, Helmholtz Centre for Environmental Research – UFZ; Leipzig, Germany.

[6]Institute of Ecology, Laboratory for Earth Surface Processes, College of Urban and Environmental Sciences, Peking University; Beijing, China.

[7]Potsdam Institute for Climate Impact Research (PIK), Member of the Leibniz Association, Potsdam, Germany.

[8]Leibniz Centre for Agricultural Landscape Research, Müncheberg, Germany.

[9]Key Laboratory of Nonpoint Source Pollution Control, Institute of Agricultural Resources and Regional Planning, Chinese Academy of Agricultural Sciences; Beijing, China.

[10]National Engineering Laboratory for Lake Pollution Control and Ecological Restoration, Chinese Research Academy of Environmental Sciences; Beijing, China.

[11]State Key Laboratory of Plant Genomics, Institute of Genetics and Developmental Biology, Chinese Academy of Sciences; Beijing, China.

[12]School of Urban Planning and Design, Peking University Shenzhen Graduate School; Shenzhen, China.

†These authors contributed equally to this work.

*Corresponding author. Email: zhouf@pku.edu.cn

Extreme climate events constitute a major risk to global food production. Among these, the extreme rainfall is often dismissed from historical analyses and future projections, whose impacts and mechanisms remain poorly understood. Here, we used long-term nationwide observations and multi-level rainfall manipulative experiments to explore the magnitude and mechanisms of extreme rainfall impacts on rice yield in China. We find that rice yield reductions due to extreme rainfall were comparable to those induced by extreme heat over the last two decades, reaching 7.6 ± 0.9% (one standard error) according to nationwide observations and 8.1 ± 1.1% according to the crop model incorporating the mechanisms revealed from manipulative experiments. Extreme rainfall reduces rice yield mainly by limiting nitrogen availability for tillering that lowers per-area effective panicles and by exerting physical disturbance on pollination that declines per-panicle filled grains. Considering these mechanisms, we projected ~8% additional yield reduction due to extreme rainfall under warmer climate by the end of the century. These findings demonstrate that it’s critical to account for extreme rainfall in food security assessments.

Main

Extreme climate events have been recognized as a major risk induced by climate change[1]. Agricultural ecosystems are among the most vulnerable to climate extremes, resulting in declines in crop production (either through yield or harvested area)[2]. For example, climate anomalies have been shown to account for as much as a third of the observed anomalies in global crop yields[3,4], with extreme events playing a particularly important role[5]. The consequences of such yield anomalies vary from fluctuations in food prices, destabilized food supply, to famines[6]. As such, understanding the impacts of extreme climate events on crop yield is critical for adapting food systems to future climate change and thus contributing to food security for the growing global populations. Recent studies have focused on elucidating impacts of drought[7,8], extreme heat[9,10] and cold spells[11], but the impact of extreme rainfall on yields remain largely uncertain[12,13].

Estimating the yield loss due to extreme rainfall needs to assess the magnitude of extreme rainfall and timing of crop exposure, both of which are highly heterogeneous over space and time. Spatially, previous studies indicate that yield statistics and climate variables aggregated at administration zones have likely smoothed out the highly localized extreme rainfall events, which could have resulted in non-significant and weaker impact of extreme rainfall than drought reported based on national statistics[2,12]. Temporarily, the exposure of crops to extreme rainfall can be dismissed if using climate data with coarse temporal resolution to explore the climate-yield relationships[12]. The lack of clear mechanistic evidence for extreme rainfall impacts has also rendered crop modelers to dismiss their potential effects in projecting the impacts of climate change[14], despite the expected increase in occurrence of extreme rainfall[15].

Rice is the primary calorie source for more than 50% of the world's population, with the largest production in China[16]. This crop is generally considered to be strongly tolerant to extreme rainfall, though this may be an artifact of relatively intense irrigation and drainage management that minimizes adverse effects of rainfall anomalies. While the impacts of extreme rainfall through secondary processes (e.g., waterlogging[17]) have been well documented, the impacts through biophysical or biochemical processes remain poorly investigated. Here, we used long-term nationwide observations and multi-level rainfall manipulative experiments to explore the magnitude and mechanisms of extreme rainfall impacts on rice yield in China. We further improved a process-based crop model by explicitly accounting for the biophysical or biochemical mechanisms to hindcast and project the yield responses to extreme rainfall across China. This combination of field observation, manipulative experiment, and model simulation enables us to address three questions here: what is the magnitude and pattern of change in rice yield due to extreme rainfall during 1999-2012? what are the key mechanisms determining rice yield response to extreme rainfall? how strongly do changes in extreme rainfall impact future rice yield?

Results

Evidence from nationwide observations

We used a window searching strategy to isolate changes in rice yield (ΔY) induced separately by an extreme climate event for each site and rice type from the nationwide observations in 1999-2012 (Methods and Supplementary Text 1), yielding 707 ΔY data at 114 sites (Supplementary Fig. 1b and data 1). While the data were by far limited and not homogeneously distributed, they represented climate heterogeneity across China's rice production areas quite well (Supplementary Text 2). These data show that extreme rainfall induced a significant yield reduction by 7.6±0.9% (one standard error) in China (n = 217, P < 0.001, Fig. 1a). Counter-intuitively, the yield reduction due to extreme rainfall was comparable to that due to extreme heat (5.4±1.7%, n = 61, P = 0.27), and larger than the reductions related to drought (4.2±1.1%, n = 152, P = 0.01), extreme cold (3.7±0.9%, n = 163, P = 0.002), and the remaining extreme events (e.g., hail, typhoon and tropical cyclones, 2.9±1.1%, n = 114, P < 0.001, Fig. 1a). The larger ΔY for extreme rainfall in relative to other extreme events was robust when comparing different extreme events with similar probability of occurrence (Supplementary Fig. 2), and was not strongly influenced by the methods used (window searching strategy versus superposed epoch analysis[2], time series analysis[13], and panel regression model[18]; Fig. 1a and Supplementary Fig. 3). Spatial analyses further confirm that the negative effects of extreme rainfall on rice yield are more pervasive and stronger than those of other extreme events, even though record yield reductions (ΔY < –20%) can arise from any type of extreme events considered here (Fig. 1b-f and Supplementary Fig. 4).

Figure. 1

To identify the potential factors determining the magnitude of extreme rainfall impacts, correlation analyses were performed between ΔY and extreme rainfall parameters. Extreme rainfall is defined as hourly precipitation exceeding the threshold that is the 99th percentile of growing-season hourly precipitation over the base period 1981–2012 for each site. An extreme rainfall event is defined as a time period that involved at least one hour with extreme rainfall and for which the break duration between hourly precipitation does not exceed 6 hours[19]. Based on the hourly precipitation data from the China Meteorological Administration (CMA), five extreme rainfall parameters were quantified during the rice growing season (Supplementary Data 1), including intensity as the maximum hourly precipitation when exceeding the threshold (cm h^{-1}), total intensity as the sum of hourly precipitation when exceeding the threshold (cm), frequency as the fraction of hours of extreme rainfall (%), proportion as the sum of hourly precipitation that exceeds the threshold divided by the growing-season total precipitation (%), and event amount as the precipitation amount averaged for extreme rainfall events (cm per event). The correlation analyses show that extreme rainfall induced ΔY was negatively correlated with intensity and event amount of extreme rainfall occurred during rice growing season, rather than with the total intensity, frequency, or proportion of extreme rainfall (Supplementary Fig. 5a). The combining results from the Kruskal-Wallis Rank Sum Test and the Dunn's test affirm that the repeated extreme rainfall does not add to additional yield loss (Supplementary Fig. 5b). These relationships are robust against variations in the definitions of extreme rainfall (exceeding 95th, 99th or 99.9th percentile of growing-season hourly precipitation over the base period) and of break duration between hourly precipitation (2, 6 or 12 hours) for consecutive extreme rainfall events (Supplementary Table 1), confirming the key driving indicators are extreme rainfall intensity and event amount rather than repeated frequencies.

The nationwide observations also indicated that rice might be more vulnerable to extreme rainfall intensity than rainfed crops. Although with large site-to-site differences, we found that rice yield was negatively affected by rainfall when intensity exceedingly around 20 cm h^{-1} (Supplementary Fig. 6). This threshold seems lower than that detected by Lesk et al.[12] on rainfed maize and soybean over the US Midwest. This is understandable since yield of largely rainfed crops may benefit from extreme rainfall by improving plant available water or buffering drought[8,20], while intensively irrigated rice benefits less from the compensating effects. More soluble nutrient loss from rice fields than that of maize and soybean also contribute to the high sensitivity to extreme rainfall[21,22].

Experimental tests of rainfall-rice yield relationship

To isolate the mechanisms leading to extreme rainfall impacts on ΔY, we established a series of rainfall manipulative experiments in 2018 and 2019 at the Jingzhou Agrometeorological Experimental Station located in Central China (Fig. 2a and

Supplementary Fig. 7). In the experiments, we established four rainfall levels of intensity and event amount to broadly represent extreme rainfall heterogeneity across China's rice fields. To test if the impacts differ by growth phases, rainfall manipulation was conducted for each or their combination of the three phases (i.e., vegetative phase when tillers are formed, reproductive phase when spikelets reach anthesis, and ripening phase when grains are filled). We quantified ΔY between treatment and control plots for which two replicates were considered, and converted the manipulative rainfall to equivalent natural rainfall in terms of measured kinetic energy (see Methods). ΔY was −1.1 ± 0.3% and −0.6 ± 0.1% in response to 1-centimeter increase in extreme rainfall intensity and event amount, respectively. These effect sizes were also statistically the same between the two experimental years (Supplementary Fig. 8a, b). Analyses of changes in yield components indicated that ΔY were mostly caused by declines in effective panicles per unit land area (EP) and filled grains per panicle (FG), accounting for 22% to 25% and 71% to 75% of ΔY, respectively, whereas decreased grain weight (GW) only contributed to approximately 1.4% to 6.0% (Fig. 2c-e and Supplementary Fig. 8c). Extreme rainfall impacts on yield components depend on growth phase: extreme rainfall in the vegetative phase mainly reduced EP, while in the reproductive phase, it mainly reduced FG. (Fig. 2c, d).

Figure. 2

The damages of extreme rainfall result from biophysical and biochemical processes, and secondary processes such as waterlogging[17], stem laydown[23], and disease development[24,25]. In our experiments, no plants were washed away, fell, or infected due to rainfall manipulation. We therefore hypothesized that the growth phase-dependent effects of extreme rainfall mainly result from biophysical and biochemical mechanisms in reducing rice yield, that is, high extreme rainfall intensity reduces per-panicle filled grains through physical disturbance (in terms of kinetic energy) on pollination[26], and high extreme rainfall event amount stresses tillering through inducing soil N losses[12]. To test these hypotheses, we conducted two supplementary experiments using the maximum rainfall level (103 mm per hour for natural rainfall intensity or 240 mm per event for event amount) in 2021 (see Methods).

In the first supplementary experiment, we sheltered half of each rice plot during the reproductive phase so that the sheltered halves of treatment were affected by extreme rainfall only through its effects on soil N losses, but not direct physical disturbance (Fig. 2a and Supplementary Fig. 9). We found FG in the sheltered halves of treatment show little difference (< 2.0%) with the control, while FG in the exposed halves of treatment decreased by 18.0 ± 2.6% (Fig. 2). The empty or shrunken grains were found mostly in the upper part of the panicles of the exposed halves of treatment (Supplementary Fig. 10), further supporting that FG were reduced by the physical disturbance that prevents successful pollination, a critical process of yield formation.

The second supplementary experiment isolates the effects of soil N losses induced by extreme rainfall event amount during the vegetative phase (Supplementary Fig. 9a). We supplied additional urea to half of the treatments, so that if there was a soil N loss induced by the extreme rainfall, it would be compensated. We found that urea re-application could help maintain N uptake per tiller, and thus successfully stabilized EP and rice yield (Fig. 2). Treatments that did not compensate for N losses caused proportionally similar declines in N uptake per tiller and thereby EP ($R^2 = 0.70$ and 0.57, respectively, $P < 0.001$, Supplementary Fig. 11). These findings confirm that the reduced EP was primarily attributable to extreme rainfall event amount that limits soil N availability and crop N uptake causing lower yields.

Figure. 3

Ultimately, we conducted a series of structural equation models (SEMs) to test potential pathways by which extreme rainfall reduces rice yield (Supplementary Fig. 12). The SEMs were formulated based on the experimental measurements of rice yield, physiological factors, physical and chemical factors in 2018 and 2019 (see Methods). The SEM including the direct pathways of rainfall-induced physical disturbance and soil N losses shows the best performance (Fig. 3), explaining 56% of the overall variance in rice yield reductions. This suggests that both pathways are primary mechanisms explaining ΔY, whereas other potential mechanisms (e.g., changes in photosynthesis, leaf area index, phosphorous loss, phosphorous and potassium absorptions) do not show significant effects (Supplementary Fig. 12b-f). In addition to these two direct pathways, the best-explaining SEM also identified an indirect pathway, i.e., rainfall-induced N losses during the vegetative phase, which may also limit per-panicle N uptake during the reproductive phase thereby decreasing FG (Fig. 3).

Crop model improvements for assessing ΔY

Correctly representing the mechanisms through which extreme rainfall reduces rice yield is critical for diagnosing and projecting spatiotemporal variations in rice yield. We introduced the physical disturbance module of extreme rainfall on rice yield in ORganizing Carbon and Hydrology in Dynamic EcosystEms for crops (ORCHIDEE-crop)[27], which is a process-based crop model including the representation of single, early and late rice types, paddy rice irrigation, and a detailed soil hydrology model[28]. The direct and indirect pathways of extreme rainfall through soil N losses was also introduced into the model (see Methods and Supplementary Table 2). The model with the extreme rainfall processes was calibrated by the experimental observations in 2018-2019, and then validated by the nationwide observations in 1999-2012. The results show that the model, in contrast to that without the extreme rainfall processes, can reproduce the rice yield variability due to year-to-year weather variations and extreme rainfall treatments (the coefficient of determination [R^2] of 0.88 in 2018 and 0.78 in 2019, Supplementary Figs 13a and b), and robustly capture the spatiotemporal heterogeneity of ΔY induced by extreme rainfall (R^2 = 0.41, Supplementary Fig. 13c).

We then used the high-resolution global precipitation measurement (GPM) datasets[29] to drive the model with the extreme rainfall processes over China in 2001-2016 (see Methods). On average, the model with the extreme rainfall processes hindcasts lower rice yields due to the extreme rainfall by 8.1 ± 1.1% (weighted by sowing area, one standard error for interannual variability) for all rice types, 8.3 ± 1.0% for single rice, 8.6 ± 1.0% for early rice, and 7.6 ± 1.3% for late rice (Supplementary Figs 14a-c). Higher ΔY were simulated eastern China and southern coastal regions which experienced higher rainfall intensities (Supplementary Figs 14a-c). Factorial model simulations show that physical disturbance induced by extreme rainfall was the most important determinant across 47-95% of rice sowing areas (Supplementary Figs 14d-f), leading to yield losses of 3.9% for single rice, 5.1% for early rice, and 4.1% for late rice. Extreme rainfall-induced N losses dominated the ΔY mainly in Anhui and Jiangsu provinces where both N application rates[30] and extreme rainfall event amount were relatively high[31] (Supplementary Figs 14h-j).

Projected impacts of future change in extreme rainfall

Since extreme rainfall was found to have significant impacts on historical rice yields, a process which was neglected in previous process-based crop model projections under climate change[32,33], we made a attempt to project the risk of future rice yield to changing extreme rainfall dynamics. We used the high-resolution climate projection by the IPSL model zoomed over China[34], which performed well in reproducing the spectral properties of rainfall including extreme events[35], to drive the model with the extreme rainfall processes under two climate scenarios (representative concentration pathways [RCP] 4.5 and 8.5; see Methods). Considering extreme rainfall impacts led to greater projected yield reductions by the end of this century (2085-2100, Fig. 4). On average, extreme rainfall induces an additional yield reduction of 7.6% (weighted by sowing area) in China on the top of other climate-change induced impacts under RCP 4.5. We then ranked the additional yield reductions in grid cells from the largest to smallest and calculated the cumulative sowing area affected by a given additional yield change, and found that the sowing areas with additional yield reduction of >7.6% accounted for 58% for early rice, 39% for single rice, and 29% for late rice (Fig. 4a). Rice is projected to suffer from extreme rainfall events the most over northeast China and southeast coastal regions (Fig. 4b-d). However, additional yield reductions were projected to be weaker under RCP 8.5 relative to RCP 4.5 (Fig. 4e-h), with the national mean reduction due to extreme rainfall of 5.4%, mainly because of larger rice yield reduction induced by stronger warming and carbon dioxide concentrations under RCP 8.5 together with no differences in projected extreme rainfall between the two scenarios (Supplementary Fig. 15). These projections highlight the increasing risk of rice yield reductions induced by extreme rainfall. There is an urgent need to consider this risk in planning climate change adaptations, such as guaranteeing N availability to maintain tillering effectiveness[36], avoiding excessive losses to the environment[30], and breeding for rainfall-tolerant rice varieties[37].

Figure. 4

Discussion

While both nationwide observations and model simulations indicated approximately 8% of rice yield lost in China due to extreme rainfall, we note that our analyses are subject to several sources of uncertainties. On the observation side, due to rigorous screening criteria to isolate extreme rainfall impacts from other extreme events, rice yield assessment has been eliminated over the Southeast Coast where extreme rainfall is strong (Supplementary Figs 1b and 16), likely underestimating the extent of extreme rainfall induced ΔY. On the modelling side, extreme rainfall intensity and event amount used for driving the historical simulations across China were from the half-hourly and 0.1-degree GPM dataset, which is well represented for but still did not fully capture the observed heaviest rainfall extremes during rice growing seasons (Supplementary Fig. 17). Thus, our estimates of extreme rainfall impact on rice yield should be viewed as a conservative assessment. Another source of uncertainty is related to the setup of our manipulative experiments. The experiments were conducted on cloudy days to mimic natural rainfall conditions, but muted the effects of secondary processes. These secondary processes may cause rice diseases and lodging that can further compound rice yield responses[13,24]. Moreover, our experiment focused on uncovering mechanisms of extreme rainfall impacts under regular management, without climatic adaptations, which introduces additional uncertainties in future projection.

Although we focused on rice yields in China that is the largest rice producer globally, attention to other rice producing regions may yield critical insights into the biogeography and generalizability of our findings. Compared to China, rice fields in South and Southeast Asia have smaller N application rates and larger fractions of rainfed rice (Supplementary Fig. 18). Extreme rainfall in these regions may lead to a lower risk of soil N losses and thus lower impacts on tillering. However, these regions were more exposed to extreme rainfall given much higher extreme rainfall intensity (Supplementary Fig. 16b), and thus subject to higher risk of physical disturbance. Since, extreme rainfall impacts results from direct physical disturbance on pollination across 70% of China's rice fields (Supplementary Figs 14j-l), rice yield reductions in South and Southeast Asia should also be significant. Previous projection of rice yield response to climate change without considering the extreme rainfall impacts (e.g., Webber et al.[14], Rosenzweig et al.[32], Jägermeyr et al.[33], Iizumi et al.[38]) have likely been overly optimistic in this regard.

The impacts of extreme rainfall on other staple crops such as wheat and maize remain to be explored. Although the magnitude and mechanistic representation of rice yield response to extreme rainfall may not be directly applicable to other crops, our research paradigm that combines field observations, manipulative experiments, and processed-based modelling is well transferable. Unlike rice, sizable fraction of upland crops were rainfed or under different irrigation-drainage systems[39]. Thus extreme rainfall effect may not be stronger than droughts, and the sensitivity of tillering and pollination processes in response to extreme rainfall may also be different from what we observed here. Therefore, a major research challenge remains to assess the global extreme rainfall impacts for all cereal crops.

Methods

Analysis of nationwide observational data

Yield change induced by extreme climate events. We collected field observations of rice yield and extreme climate events from the national agrometeorological observation network that is run by the CMA. This network covers the rice fields for single rice in Northeast and Central China and early and late rice in South China. All sites in the network refer to irrigated rice systems which accounts for 99% of rice fields in China (Supplementary Fig. 18). The network observed extreme climate events occurring in the rice growing seasons over the period 1999-2012 at 356 sites, but only 166 of them provide information for rice yields over the same period. In total, it provides rice yield of 2,304 observations and extreme climate events of 8,595 observations. Rice yield is defined as actual production divided by the hectare of harvested area. Extreme climate events are recorded on given days for each site and are sorted into five broad categories, i.e., extreme heat, extreme cold, extreme rainfall, drought, and the other events (see definitions in Supplementary Table 3).

We used a window searching strategy to quantify the change in rice yield (ΔY) induced by each extreme climate event. ΔY is defined as the relative difference in yield between the treatment and control cases (in %) from the same site and rice type, where in the treatment rice has been exposed to a given extreme event, and in the control rice has not been exposed to that event and other extreme events either did not occur or were the same as in the treatment. As such control and treatment pairs are from the same site with the same rice type, but different years. We adopted a 7-year moving window[2] to identify all available control-treatment pairs from the nationwide observations, yielding 707 pairs from 114 sites for quantifying the difference between control and treatment (Supplementary Fig. 1b and Data 1). However, the difference for each pair can also be attributed to changes in rice cultivar, phenology, and the interannual variations in climate condition. As such, we detrended rice yield to exclude the effects from changes in rice cultivar and phenology, and then used a panel regression model to exclude the effects from interannual weather variability. Subsequently, we isolated ΔY related to each extreme climate event for each site and rice type as follow:

$$\Delta \mathrm{Y}_{i,t,u,m} = \frac{\left(YT_{i,t,u,m}^{de} - YT_{i,t,u,m}^{fit}\right) - \left(\overline{YC}_{i,k,u,m}^{de} - \overline{YC}_{i,k,u,m}^{fit}\right)}{\overline{YC}_{i,k,u,m}^{de}} \times 100\%, \quad (1)$$

where *t*, *k*, *i*, *u*, and *m* refer to year of the treatment, year of the control, site, rice type, and event type, respectively. $YT_{i,t,u,m}^{de}$ refers to the detrended yield in the treatment. $YT_{i,t,u,m}^{fit}$ refers to fitted yield after excluding effect of inter-annual climate variation in the treatment. $\overline{YC}_{i,k,u,m}^{de}$ and $\overline{YC}_{i,k,u,m}^{fit}$ refer to the mean rice yield in the control after being detrended and fitted, respectively, if identifying multiple controls. The detailed methods are provided in Supplementary Text 1 with examples in Supplementary Fig. 19.

The t-test was applied to estimate the significance of the difference in ΔY between extreme rainfall and other extreme events. To ensure that the unequal sample size of different extreme events did not affect the significance estimates, we ran a bootstrap t-test with 1000 replicates using the R package MKinfer v.0.5. In addition, we calculated the percentiles of the extreme events occurred in year of the treatment relative to the base period 1981–2012, and found that most of them exceed 95th percentile (Supplementary Fig. 2a-d). However, these percentiles are not completely consistent among the events. To test the robustness of the differences in ΔY, we compared the effects of different extreme events with similar percentiles, that is, 95th to 99th (or 99th to 99.8th) percentiles for extreme heat and rainfall and 1st to 5th (or 0.2nd to 1st) percentiles for extreme cold and drought (Supplementary Fig. 2e-f).

Correlation between ΔY and extreme rainfall parameters. We conducted correlation analyses of the extreme rainfall induced ΔY against five parameters to identify the potential factors determining the magnitude of extreme rainfall impacts. Besides, the Kruskal-Wallis Rank Sum Test and the Dunn's test were applied to test if ΔY is sensitive to the repeated extreme rainfall (1, 2, 3 and ≥4 times). We also tested if ΔY in response to extreme rainfall is dependent on the definitions of extreme rainfall based on different thresholds (95th, 99th or 99.9th percentile) and of extreme rainfall event based on break duration (≤ 2, 6, or 12 hours) (Supplementary Table 1).

Rainfall manipulative experiments

Plants and cultivation condition. The experimental site is at the Jingzhou Agrometeorological Experimental Station in Hubei province, China (30°21′N, 112°09′E; Supplementary Fig. 7a). It is characterized as subtropical humid monsoon climate, with a mean air temperature of 16 °C and a mean precipitation of 1,095 mm yr^{-1}. Soil is classified as Hydragric Anthrosol (Supplementary Table 4). Rice seedling nurseries were managed under the water regime of continuous flooding. Seedlings of rice (*Oryza sativa* L.) were transplanted at 30-day seedling ages with a hill spacing of 0.33×0.33 m (9 hills m^{-2}), and harvested after 103 days. Rice fields were managed using yield-oriented optimal fertilizer applications. Further details on cultivation condition can be found in Supplementary Fig. 7b.

Main experiment. The rainfall manipulative experiment was conducted from 2018 to 2019, spanning two rice growing seasons. The experiment consisted of ambient control and factorial treatments with two replicates, and was designed for extreme rainfall level-timing combinations (Supplementary Fig. 7c), with the results in Supplementary Data 1. The treatments comprised four levels of extreme rainfall intensity and event amount in each or all of the three growth phases (i.e., vegetative, reproductive, and ripening phases), as they impact crop yield through different mechanisms. For instance, the extreme rainfall with high intensity damage plant tissue[40]; whereas that with large event amount limits crop uptake through increasing soluble nutrient losses and waterlogging[12,17]. There was a total of 34 plots, each of which had an area of 6 m^2 (2 m × 3 m) and was completely isolated by plastic-covering levees and impervious plates at a 0.5-meter distance in between. Throughout the experiment, all plots were subjected to the same agricultural management practices. To avoid the border effects, we use independent-samples t-test to compare the yield of ambient control with that of three plots nearby, with each plot owing 150 m^2 (25 m × 6 m) with the same agricultural management practices, and found no significant differences during three rice growing seasons (*P* >0.05, Supplementary Fig. 20a).

We manipulated rainfall levels by running the artificial rainfall manipulation system (NLJY-10, Nanlin Electronics, China) for one hour on two replicates for each treatment, with the rainfall amount of 60, 120, 180, and 240 mm. For more consistent estimates on the extreme rainfall impacts in both the field and the experiment, we thus measured the kinetic energy of manipulative rainfalls using the laser precipitation disdrometer (OTT Parsivel^2, Hach, USA), which is equivalent to the natural rainfall intensities of 6, 19, 51, and 103 mm per hour[41,42]. These rainfall levels represent most of the broad range of growing-season rainfall extremes (exceeding the 99th percentile) across China's rice fields (i.e., 8 to 143 mm per hour and 12 to 526 mm per event observed during1999-2012). To approximate the natural rainfall condition, rainfall manipulation was conducted in cloudy daytime for vegetative and ripening phases, but for reproductive phase specifically at 8:00-13:00 when spikelets reach anthesis in experimental site. To minimize the impact of waterlogging, ponded water was discharged within 12 hours after rainfall manipulation if the depth exceeds 100 mm.

For each plot, we measured leaf area index, total tiller number, dry weights of leave, stem, and panicle, which were determined from three hills with an average number of tillers (Supplementary Data 1). All leaves, stems, and panicles were oven-dried (DHG500, SUPO Co.) at 75°C for at least 72 h, before analyzing N, P, and K contents using a continuous flow analyzer (Elementar, Germany). We measured net photosynthesis of three flag leaves at two photosynthetic photon flux densities of 1500 and 600 μmol m^{-2} s^{-1} using Li6400 (Li-Cor Inc., USA). These measurements were conducted at seedling, maturity, and during three growth phases. Net photosynthesis was measured before and after each rainfall manipulation. In addition, for each treatment, we observed N and P losses via runoff and leaching during the period from the beginning of rainfall manipulation to the time when ponded water level decreased the same as that before manipulation.

At maturity, three hills with an average number of panicles were collected from each plot to determine the yield estimated as the product of effective panicles per unit land area (EP), filled grains per panicle (FG), and grain weight (GW) (Supplementary Data 1). The filled grains were oven-dried at 75 °C for at least 72 h, but their weights were adjusted to a fresh weight with a moisture content of 0.15 g H_2O g^{-1}, ref[43]. To determine actual yields, the filled grains from the other rice plant hills for all plots were machine-threshed (OUGEDA Co., China) and sun-dried to reach a moisture content of 0.15 g H_2O g^{-1}. The yields for all plots were highly consistent with actual ones (Supplementary Fig. 20b-c).

We calculated relative changes in rice yield and in yield components between the controls and treatments (ΔY, ΔEP, ΔFG, and ΔGW in %) to simplify comparisons among treatments. Note that the compensation relationship between ΔEP and ΔFG can be avoided in our experimental plots as rice planting distance is 30 cm (ref[44]). ΔY is equal to the sum of ΔEP, ΔFG, and ΔGW, that is ΔY = ΔEP + ΔFG + ΔGW according to the Kaya identity principle[45]. The attribution results help identify the key yield components that were most affected by extreme rainfall. We further identified in which growth phase extreme rainfall regulates the changes in key yield components.

1st supplementary experiment. To isolate the mechanism driving the causal relationship between extreme rainfall and ΔFG, we ran the first supplementary experiment during the reproductive phase in July 2021. In the experiment, extreme rainfall intensity is 103 mm per hour (Supplementary Fig. 9 and Data 1). For each treatment, transparent impervious film was placed above half of the plot, such that half of the plants were fully exposed to artificial rainfall and the other part was sheltered but experienced the same increases in ponded water levels and nutrient losses as the exposed part. To avoid an unintentional influence of film on rice growth, the film was also placed above a half control plots and all films were removed when the experiment ended.

FG and actual yield in exposed and sheltered parts for each plot were observed. Based on the observations, we attributed the effect of extreme rainfall on ΔFG into physical disturbance and soil N loss as below:

$$\text{Total: } \Delta Y = Y_{ROC} - Y_{COC},\ \Delta FG = FG_{ROC} - FG_{COC}, \tag{2a}$$

$$\text{Soil N loss } (o)\text{: } \Delta Y_o = Y_{RC} - Y_{CC},\ \Delta FG_o = FG_{ROC} - FG_{COC}, \quad (2b)$$

$$\text{Physical disturbance } (p)\text{: } \Delta Y_p = \Delta Y - \Delta Y_o,\ \Delta FG_p = \Delta FG - \Delta FG_o, \quad (2c)$$

where *ROC* and *COC* refer to the exposed parts for treatment and control, respectively. *RC* and *CC* refer to the sheltered parts for treatment and control, respectively. In addition, we measured the number of empty and shrunken grains at maturity as well as their distribution along panicle. Such observations elucidate how extreme rainfall influences rice pollination during reproductive phase.

2nd supplementary experiment. To confirm the causal effect of extreme rainfall on ΔEP, we ran the second supplementary experiment during vegetative phase in June 2021. The experiment consisted of ambient control and two treatments with rainfall amount of 240 mm (Supplementary Fig. 9a and Data 1). For treatments, rice plants were fully exposed to artificial rainfall on 6 plots, half of which were re-applied by 28.8 kg N ha^{-1} (37% of tillering fertilizer application) in the form of urea after rainfall manipulation. The re-application rate was determined as the average of observed N losses from the treatment plots using the same rainfall amount during vegetative phase in 2018 and 2019.

For each plot, we observed EP and the actual yield at maturity as well as N uptake per tiller from transplantation to panicle initiation, and tested their differences between treatments and controls using the Wilcoxon rank sum test. If no significant differences between N re-applied treatment and control but significant differences between normal treatment and control were found, the decrease in EP were attributed to N losses induced by extreme rainfall during the vegetative phase.

Path analysis. Structural equation modelling (SEM) implemented in the R package 'lavaan 0.6-7' allows us to test different pathways by which extreme rainfall affects rice yield. On the basis of potential causal relationships revealed by our experiments and previous literatures[12,26,46], SEMs were formulated based on the experimental measurements of rice yield parameters (i.e., actual yield, effective panicles per unit land area, filled grains per panicle, and grain weight), physiological factors (i.e., leaf area index, total tiller number, aboveground dry weights, N, P, and K uptakes, net photosynthesis), and physical and chemical factors (kinetic energy of rainfall, N and P losses via runoff and leaching) in 2018 and 2019. The insignificant paths ($P > 0.05$) were eliminated gradually until all links significantly contributed to the final model. To compare model performance, we conducted a chi-squared difference test and calculated model fit statistics (root mean square error of approximation [RMSEA], comparative fit index [CFI], goodness-of-fit index [GFI] and adjusted R squared [R^2_{adj}]). Standardized path coefficients were computed according to ref.[47], which can be interpreted as the change in the dependent variable when the independent variable changes by one standard deviation.

Process-based modelling for regional assessments

We improved the process-based crop model ORCHIDEE-crop[27,28,48] to account for direct and indirect pathways of extreme rainfall revealed by the best-explaining SEM. We then used the model with the extreme rainfall processes to hindcast and project the impacts of extreme rainfall on rice yield across China during 2001-2016 and 2085-2100 under two Representative Concentration Pathways (RCP 4.5 and 8.5).

Model improvement. ORCHIDEE-crop simulates crop phenology, leaf area dynamics, growth of reproductive organs, carbon allocation and managements, as well as carbon, water and energy fluxes of agroecosystems. This model has been applied globally and regionally, and found to robustly reproduce yield variability[49]. ORCHIDE-crop is suitable for this study since it has been optimized for simulating the phenology and yield of single, early and late rice types in China[27,48]. It has paddy irrigation and soil hydrology schemes[28], able to represent the typical irrigation and drainage systems for China's rice fields. It runs in a half-hourly time-step and at 0.5-degree grid cell, suitable for extreme rainfall of short duration, which is a challenging issue for the models running at daily time-step.

In ORCHIDEE-crop, the rice growth starts from transplanting, and the growth cycle includes three stages divided by the onset of grain filling and the physiological maturity[48]. Starting from grain filling, the quantity of dry matters accumulated in grains is calculated by applying a progressive "harvest index" to the biomass of the plant. The daily rate of grain increment is proportional to the daily accumulated thermal unit, which could be reduced by frost and extreme heat[50]. The impacts of extreme rainfall are formulated as a factor (α) to reduce the rate of grain increment:

$$\alpha = (1 + \Delta EP + \Delta FG), \tag{3a}$$

$$\Delta EP = 0.262 \cdot \Delta N_{ut} - 1.644, \tag{3b}$$

$$\Delta FG = -0.00424 \cdot KE_{re} - 0.00115 \cdot KE_{ri} + 0.139 \cdot \Delta N_{up} - 3.676. \tag{3c}$$

These model equations were derived from the best-explaining SEM, where ΔN_{ut} and ΔN_{up} denote relative change in N uptake per tiller and N uptake per panicle during vegetative phase (%) as a function of soil N losses, respectively. KE_{re} denotes kinetic energy (J m^{-2} h^{-1}) of the maximum hourly precipitation (exceeding the 99th percentile) occurred at 8:00-16:00 in flowering period when spikelets reach anthesis and if hourly air temperature ranges from 23°C to 35°C, ref[51,52]. KE_{ri} denotes kinetic energy of the maximum hourly precipitation (exceeding the 99th percentile) during ripening phase. Note that Equation 3 summing ΔEP and ΔFG is suitable to diagnose and project extreme rainfall induced ΔY across China, since the rice planting distances of 17 to 25 cm in China are enough to avoid the compensation relationship between EP and FG[44] (Supplementary Data 1). Further details on model equations can be found in Supplementary Table 2.

Historical simulation. Two sets of historical simulations were performed for three rice types over China: (1) the comprehensive simulation (S0) that accounts both impacts of rainfall-induced physical disturbance and soil N losses on rice yield and (2) the partial simulation (S1) that only accounts the impact of physical disturbance. By comparing S0 and S1, we isolate the impact of soil N losses. The difference between yield simulations from simulation with and without the extreme rainfall processes can be attributed to the historical extreme rainfall (Supplementary Data 2), thus we derived ΔY as below:

$$\Delta Y = \frac{Yield\ simulation_{with} - Yield\ simulation_{without}}{Yield\ simulation_{without}} \times 100\%. \quad (4)$$

Details on historical input data can be found in Supplementary Table 5. Specifically, we used field observed rice phenology from the CMA to interpolate 0.1-degree transplanting date[48]. We used the satellite-based gridded precipitation datasets (GPM IMERGv6) to quantify extreme rainfall intensities and event amounts, since it is well represented at the site scale (Supplementary Fig. 17).

Future projections. To evaluate the implications of our findings for future rice yield projections over China, we applied the ORCHIDEE-crop model with the extreme rainfall processes to simulate yield changes of three rice types under RCP 4.5 and 8.5 with present-day agricultural management practices (Supplementary Data 2). To analyze the effect of future extreme rainfall on rice yield, we estimated additional rice yield loss as the difference between yield simulations with and without the extreme rainfall processes in 2085-2100 divided by the yield simulation without the extreme rainfall processes in 2001-2016. To remove systematic deviations of the simulated historical climate, we applied the trend-preserving bias-correction[53] to the IPSL projected climate change[34]. The bias correction was then applied to the climate forcing data and extreme rainfall indices during 2085-2100. Further details on input data source for future projections can be found in Supplementary Table 5.

Data availability: The data from the national agrometeorological observation network and the rainfall manipulative experiments are available in Supplementary Data 1. The climate data, records of extreme climate events, rice yield and phenology at the site scale from the China Meteorological Administration (CMA) are available at https://data.cma.cn/en. Model input data for historical simulations and future projections are available from public data depositories listed in Supplementary Table 5. The global precipitation measurement (GPM) IMERGv6 are available at https://disc.gsfc.nasa.gov/datasets/GPM_3IMERGHH_06/summary. Model output data for historical simulations and future projections are available in Supplementary Data 2. Source data are provided with this paper.

Code availability: Source codes for data analyses are available from https://www.doi.org/10.6084/m9.figshare.19801765. Source codes for process-based model are available from http://forge.ipsl.jussieu.fr/orchidee, under the French Free Software license, compatible with the GNU GPL (http://cecill.info/licences.en.html).

Acknowledgements

This study was supported by the National Natural Science Foundation of China (42225102, 41977082, F.Z.; 42007079, J.F.; 42171096, X.H.W.; 41530528, S.L.P). We acknowledge Kaiwen Liu, Jianping Wang and Lanying Shu from Jingzhou Agrometeorological Experimental Station, Sheng Wang, Wulahati Adalibieke, Yan Bo, Changxian Wu, Wenjun Jiang, Meishuai Yuan, Hongwei Cai, and Chengjie Wang from Peking University, Xinyi Huang, Lian Chen and Daoheng Zhuang from Central China Normal University, Chunshan Li from South China Sea Institute of Oceanography, Chinese Academic of Science for supporting field experiments and laboratory analyses. We acknowledge the CMA for nationwide observations of rice yield, phenology, hourly precipitation, and extreme climate events, the NASA for GPM IMERGv6 data.

Author contributions

F.Z. designed the study. Y.W.J., J.F. and X.H.W. performed all computational analyses. F.Z., X.H.W., J.F. and Y.W.J. drafted the paper. L.L. provided high-resolution climate projection using the IPSL model. All co-authors reviewed and commented on the manuscript.

Competing interests

The authors declare no competing interests.

Figure captions

Fig. 1. Changes in rice yield (ΔY) induced by extreme climate events in China. **a**. ΔY (mean ± standard error) quantified by the window searching strategy (left column of each pair) and mean of three other methods[2,13,18] (right column of each pair, n = 3, see Supplementary Text 1). Asterisks refer to statistical significance of the differences in mean ΔY between extreme rainfall and other events based on the two-sided bootstrap t-test, with * $P < 0.05$, ** $P < 0.01$, *** $P < 0.001$, and n.s. for not significant. For left column of each pair, n = 217 for extreme rainfall, n = 61 for extreme heat, n = 152 for drought, n = 163 for extreme cold, and n = 114 for the other events. **b-f**. Patterns of ΔY induced by extreme rainfall at 82 sites, extreme heat at 18 sites, drought at 73 sites, extreme cold at 61 sites, and the other events at 68 sites (typhoon and tropical cyclones), respectively. Each point in panels **b** to **f** represents the location of a given extreme climate event with ΔY, with size of the symbols showing the mean percent change over the period 1999-2012. The base map of the country boundaries was from the Global Administrative Areas dataset (https://gadm.org).

Fig. 2. Effects of simulated rainfall on rice yield and yield components. **a**. Experimental setup. **b** to **e**. Relative changes in rice yield (ΔY), effective panicles per unit land area (ΔEP), filled grains per panicle (ΔFG), and grain weight (ΔGW), respectively. For the 2^{nd} supplementary experiment, the urea re-application rate (i.e., 28.8 kg N ha^{-1}) is equal to the average N losses observed from the treatment plots using the same rainfall amount during vegetative phase in main experiments. Sample size is

4 for each treatment, but 3 for each supplementary experiment. Data are presented as mean ± standard error. Asterisk indicates for the significant difference with zero based on two-sided t-test, with $P < 0.05$.

Fig. 3. Schematic diagram of extreme rainfall impacts on rice yield. Best-explaining SEM illustrating major pathways through which extreme rainfall reduced rice yield ($\chi^2 = 22.8$, $P = 0.530$, df = 24, n = 32). Single-headed arrows indicate the direction of causation identified by the structural equation modelling. Blue (red) arrows indicate significant positive (negative) effects ($P < 0.05$). Arrow width is proportional to the strength of the relationship, which is characterized by standardized path coefficients showing next to arrows. The coefficients can be interpreted as the change in the dependent variable when the independent variable changes by one standard deviation. $Amount_{veg}$, extreme rainfall event amount in vegetative phase; $Intensity_{rep}$ and $Intensity_{rip}$, extreme rainfall intensity in reproductive and ripening phases, respectively; ΔY, relative changes in rice yield.

Fig. 4. Future projections of additional yield change induced by extreme rainfall. **a** and **e.** Cumulative proportions of sowing area affected by a given additional yield change under RCP 4.5 and RCP 8.5, respectively; Black dashed lines represent the national means (−7.6% and −5.4%), and the numbers represent the cumulative proportions of sowing area affected by exceeding the national means. **b** to **d**. Patterns of ΔY under RCP 4.5. **f** to **h**. Same as panels **b** to **d** but under RCP 8.5. The base map

of the country boundaries was from the Global Administrative Areas dataset (https://gadm.org).

References

1 IPCC. *Managing the Risks of Extreme Events and Disasters to Advance Climate Change Adaptation. A Special Report of Working Groups I and II of the Intergovernmental Panel on Climate Change [Field, C.B., V. Barros, T.F. Stocker, D. Qin, D.J. Dokken, K.L. Ebi, M.D. Mastrandrea, K.J. Mach, G.-K. Plattner, S.K. Allen, M. Tignor, and P.M. Midgley (eds.)].* (Cambridge University Press, 2012).

2 Lesk, C., Rowhani, P. & Ramankutty, N. Influence of extreme weather disasters on global crop production. *Nature* **529**, 84-87, doi:10.1038/nature16467 (2016).

3 Ray, D. K., Gerber, J. S., MacDonald, G. K. & West, P. C. Climate variation explains a third of global crop yield variability. *Nat Commun* **6**, 5989, doi:10.1038/ncomms6989 (2015).

4 Proctor, J., Rigden, A., Chan, D. & Huybers, P. More accurate specification of water supply shows its importance for global crop production. *Nat Food* **3**, 753–763, doi:10.1038/s43016-022-00592-x (2022).

5 Vogel, E. *et al.* The effects of climate extremes on global agricultural yields. *Environ Res Lett* **14**, 054010, doi:10.1088/1748-9326/ab154b (2019).

6 Hasegawa, T. *et al.* Extreme climate events increase risk of global food insecurity and adaptation needs. *Nat Food* **2**, 587-595, doi:10.1038/s43016-021-

00335-4 (2021).

7 Lobell, D. B. *et al.* Greater Sensitivity to Drought Accompanies Maize Yield Increase in the US Midwest. *Science* **344**, 516-519, doi:10.1126/science.1251423 (2014).

8 Lesk, C. *et al.* Stronger temperature-moisture couplings exacerbate the impact of climate warming on global crop yields. *Nat Food* **2**, 683-691, doi:10.1038/s43016-021-00341-6 (2021).

9 Wang, X. H. *et al.* Emergent constraint on crop yield response to warmer temperature from field experiments. *Nat Sustain* **3**, 908-916, doi:10.1038/s41893-020-0569-7 (2020).

10 Lobell, D. B., Sibley, A. & Ortiz-Monasterio, J. I. Extreme heat effects on wheat senescence in India. *Nat Clim Change* **2**, 186-189, doi:https://doi.org/10.1038/nclimate1356 (2012).

11 Zhang, J. Y., Li, X. M., Lin, H. X. & Chong, K. Crop Improvement Through Temperature Resilience. *Annu Rev Plant Biol* **70**, 753-780, doi:10.1146/annurev-arplant-050718-100016 (2019).

12 Lesk, C., Coffel, E. & Horton, R. Net benefits to US soy and maize yields from intensifying hourly rainfall. *Nat Clim Change* **10**, 819-822, doi:10.1038/s41558-020-0830-0 (2020).

13 Li, Y., Guan, K. Y., Schnitkey, G. D., DeLucia, E. & Peng, B. Excessive rainfall leads to maize yield loss of a comparable magnitude to extreme drought in the United States. *Global Change Biol* **25**, 2325-2337, doi:10.1111/gcb.14628

(2019).

14 Webber, H. *et al.* Diverging importance of drought stress for maize and winter wheat in Europe. *Nat Commun* **9**, 1-10, doi:https://doi.org/10.1038/s41467-018-06525-2 (2018).

15 Seneviratne, S. I. *et al. Weather and Climate Extreme Events in a Changing Climate. In: Climate Change 2021: The Physical Science Basis. Contribution of Working Group I to the Sixth Assessment Report of the Intergovernmental Panel on Climate Change.* (Cambridge University Press, 2021).

16 FAOSTAT, *Crops and livestock products*, Food and Agriculture Organization of the United Nations (FAO) (2019), Date accessed: 20th September 2019, http://www.fao.org/faostat/en/#home.

17 Shaw, R. E. & Meyer, W. S. Improved Empirical Representation of Plant Responses to Waterlogging for Simulating Crop Yield. *Agron J* **107**, 1711-1723, doi:10.2134/agronj14.0625 (2015).

18 Zhu, P. *et al.* The critical benefits of snowpack insulation and snowmelt for winter wheat productivity. *Nat Clim Change* **12**, 485-490, doi:10.1038/s41558-022-01327-3 (2022).

19 Wu, X. S. *et al.* On the event-based extreme precipitation across China: Time distribution patterns, trends, and return levels. *J Hydrol* **562**, 305-317, doi:10.1016/j.jhydrol.2018.05.028 (2018).

20 Lesk, C. *et al.* Compound heat and moisture extreme impacts on global crop yields under climate change. *Nat Rev Earth Env* **3**, 872-889,

doi:10.1038/s43017-022-00368-8 (2022).

21 Hou, X. K. *et al.* Detection and attribution of nitrogen runoff trend in China's croplands. *Environ Pollut* **234**, 270-278 (2018).

22 Gao, S. S. *et al.* Quantifying nitrogen leaching response to fertilizer additions in China's cropland. *Environ Pollut* **211**, 241-251, doi:10.1016/j.envpol.2016.01.010 (2016).

23 Steiner, J. L., Briske, D. D., Brown, D. P. & Rottler, C. M. Vulnerability of Southern Plains agriculture to climate change. *Climatic Change* **146**, 201-218, doi:10.1007/s10584-017-1965-5 (2018).

24 Mäkinen, H. *et al.* Sensitivity of European wheat to extreme weather. *Field Crop Res* **222**, 209-217, doi:https://doi.org/10.1016/j.fcr.2017.11.008 (2018).

25 Reichstein, M. *et al.* Climate extremes and the carbon cycle. *Nature* **500**, 287-295, doi:https://doi.org/10.1038/nature12350 (2013).

26 Win, A., Tanaka, T. S. T. & Matsui, T. Panicle inclination influences pollination stability of rice (Oryza sativa L.). *Plant Prod Sci* **23**, 60-68, doi:10.1080/1343943x.2019.1698971 (2020).

27 Wang, X. H. *Impacts of environmental change on rice ecosystems in China: Development, optimization and application of ORCHIDEE-CROP model (Ph.D. Thesis)*, Peking University, (2016).

28 Yin, Z. *et al.* Improvement of the Irrigation Scheme in the ORCHIDEE Land Surface Model and Impacts of Irrigation on Regional Water Budgets Over China. *J Adv Model Earth Sy* **12**, e2019MS001770,

doi:https://doi.org/10.1029/2019MS001770 (2020).

29 Huffman, G. J., Stocker, E. F., Bolvin, D. T., Nelkin, E. J. & Tan, J., *GPM IMERG Final Precipitation L3 Half Hourly 0.1 degree x 0.1 degree V06, Greenbelt, MD*, Goddard Earth Sciences Data and Information Services Center (GES DISC) (2019), Date accessed: 5th August 2021, https://disc.gsfc.nasa.gov/datasets/GPM_3IMERGHH_06/summary.

30 Cui, X. Q. *et al.* Global mapping of crop-specific emission factors highlights hotspots of nitrous oxide mitigation. *Nat Food* **2**, 886-893, doi:10.1038/s43016-021-00384-9 (2021).

31 Jian, Y. W., Fu, J., Li, B. G. & Zhou, F. Increased extreme hourly precipitation over China's rice paddies from 1961 to 2012. *Sci Rep-Uk* **10**, 10609, doi:https://doi.org/10.1038/s41598-020-67429-0 (2020).

32 Rosenzweig, C. *et al.* Assessing agricultural risks of climate change in the 21st century in a global gridded crop model intercomparison. *P Natl Acad Sci USA* **111**, 3268-3273, doi:10.1073/pnas.1222463110 (2014).

33 Jägermeyr, J. *et al.* Climate impacts on global agriculture emerge earlier in new generation of climate and crop models. *Nat Food* **2**, 873-885, doi:10.1038/s43016-021-00400-y (2021).

34 Yang, H., Jiang, Z. H. & Li, L. Biases and improvements in three dynamical downscaling climate simulations over China. *Clim Dynam* **47**, 3235-3251, doi:10.1007/s00382-016-3023-9 (2016).

35 Chen, W. L., Jiang, Z. H., Li, L. & Yiou, P. Simulation of regional climate

change under the IPCC A2 scenario in southeast China. *Clim Dynam* **36**, 491-507, doi:10.1007/s00382-010-0910-3 (2011).

36 Barbier, F. F., Dun, E. A., Kerr, S. C., Chabikwa, T. G. & Beveridge, C. A. An Update on the Signals Controlling Shoot Branching. *Trends Plant Sci* **24**, 220-236, doi:10.1016/j.tplants.2018.12.001 (2019).

37 Bailey-Serres, J., Parker, J. E., Ainsworth, E. A., Oldroyd, G. E. D. & Schroeder, J. I. Genetic strategies for improving crop yields. *Nature* **575**, 109-118, doi:10.1038/s41586-019-1679-0 (2019).

38 Iizumi, T. *et al.* Prediction of seasonal climate-induced variations in global food production. *Nat Clim Change* **3**, 904-908, doi:https://doi.org/10.1038/nclimate1945 (2013).

39 Meier, J., Zabel, F. & Mauser, W. A global approach to estimate irrigated areas - a comparison between different data and statistics. *Hydrol Earth Syst Sc* **22**, 1119-1133, doi:10.5194/hess-22-1119-2018 (2018).

40 Lepore, C., Allen, J. T. & Tippett, M. K. Relationships between Hourly Rainfall Intensity and Atmospheric Variables over the Contiguous United States. *J Climate* **29**, 3181-3197, doi:10.1175/Jcli-D-15-0331.1 (2016).

41 Atlas, D., Srivastava, R. C. & Sekhon, R. S. Doppler Radar Characteristics of Precipitation at Vertical Incidence. *Rev Geophys* **11**, 1-35, doi:DOI 10.1029/RG011i001p00001 (1973).

42 Higashino, M. & Stefan, H. G. Modeling the effect of rainfall intensity on soil-water nutrient exchange in flooded rice paddies and implications for nitrate

fertilizer runoff to the Oita River in Japan. *Water Resour Res* **50**, 8611-8624, doi:10.1002/2013wr014643 (2014).

43 Yoon, D. K. *et al.* Transgenic rice overproducing Rubisco exhibits increased yields with improved nitrogen-use efficiency in an experimental paddy field. *Nat Food* **1**, 134-139, doi:10.1038/s43016-020-0033-x (2020).

44 Gravois, K. A. & Helms, R. S. Effect of Uneven Emergence on Rice Yield, Milling Yield, and Yield Components. *Aust J Exp Agr* **34**, 949-952, doi:Doi 10.1071/Ea9940949 (1994).

45 Wang, S. A. *et al.* Reduced sediment transport in the Yellow River due to anthropogenic changes. *Nat Geosci* **9**, 38-41, doi:10.1038/Ngeo2602 (2016).

46 Ishibashi, M. & Terashima, I. Effects of Continuous Leaf Wetness on Photosynthesis - Adverse Aspects of Rainfall. *Plant Cell Environ* **18**, 431-438, doi:10.1111/j.1365-3040.1995.tb00377.x (1995).

47 Bollen, K. A. Total, direct, and indirect effects in structural equation models. *Sociological Methodology* **17**, 37-69, doi:10.2307/271028 (1987).

48 Wang, X. H. *et al.* Management outweighs climate change on affecting length of rice growing period for early rice and single rice in China during 1991-2012. *Agr Forest Meteorol* **233**, 1-11, doi:10.1016/j.agrformet.2016.10.016 (2017).

49 Müller, C. *et al.* Global gridded crop model evaluation: benchmarking, skills, deficiencies and implications. *Geosci Model Dev* **10**, 1403-1422, doi:10.5194/gmd-10-1403-2017 (2017).

50 Wu, X. *et al.* ORCHIDEE-CROP (v0), a new process-based agro-land surface

model: model description and evaluation over Europe. *Geosci Model Dev* **9**, 857-873, doi:10.5194/gmd-9-857-2016 (2016).

51 Kobayasi, K., Matsui, T., Yoshimoto, M. & Hasegawa, T. Effects of Temperature, Solar Radiation, and Vapor-Pressure Deficit on Flower Opening Time in Rice. *Plant Prod Sci* **13**, 21-28, doi:10.1626/pps.13.21 (2010).

52 Julia, C. & Dingkuhn, M. Variation in time of day of anthesis in rice in different climatic environments. *Eur J Agron* **43**, 166-174, doi:10.1016/j.eja.2012.06.007 (2012).

53 Hempel, S., Frieler, K., Warszawski, L., Schewe, J. & Piontek, F. A trend-preserving bias correction - the ISI-MIP approach. *Earth Syst Dynam* **4**, 219-236, doi:10.5194/esd-4-219-2013 (2013).

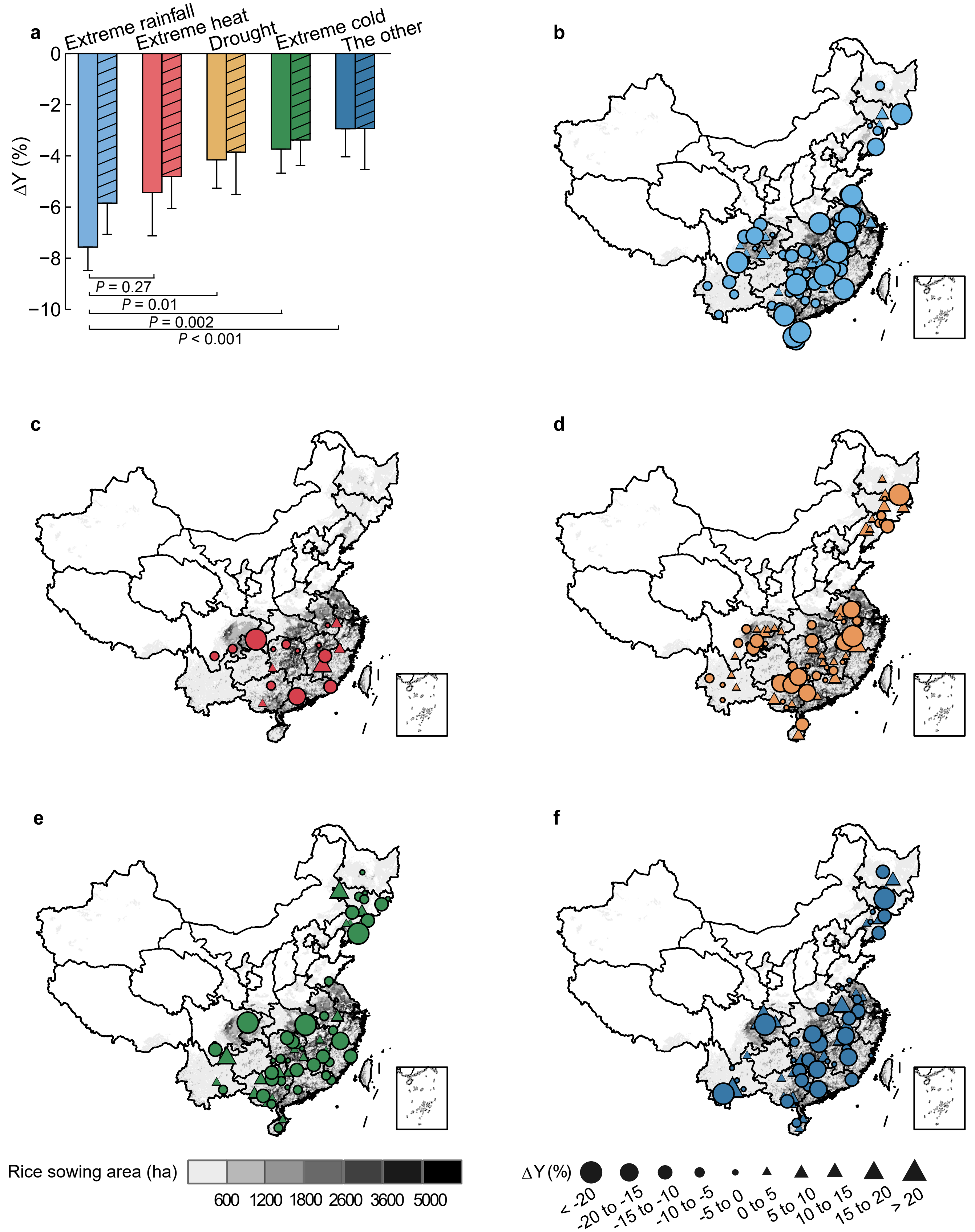
a
Extreme rainfall
Extreme heat
Drought
Extreme cold
The other
ΔY (%)
0
−2
−4
−6
−8
−10
P = 0.27
P = 0.01
P = 0.002
P < 0.001
b
c
d
e
f
Rice sowing area (ha)
600
1200
1800
2600
3600
5000
ΔY (%)
< -20
-20 to -15
-15 to -10
-10 to -5
-5 to 0
0 to 5
5 to 10
10 to 15
15 to 20
> 20

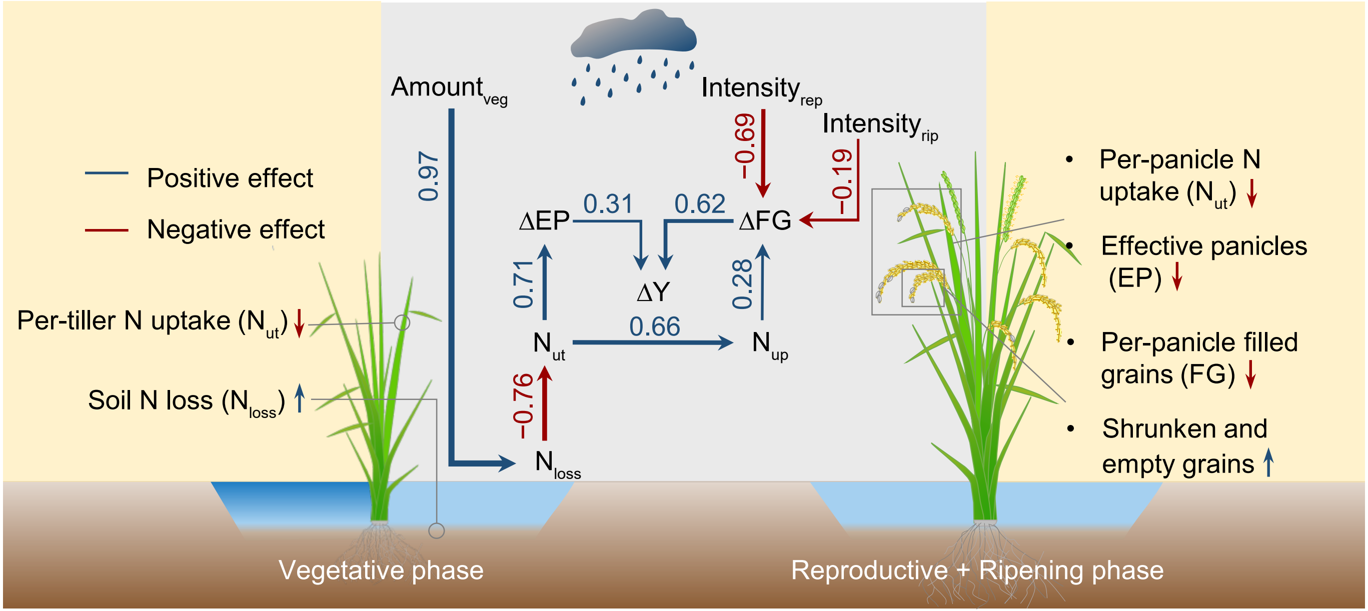

Positive effect
Negative effect
Amount$_{veg}$
Intensity$_{rep}$
Intensity$_{rip}$
0.97
−0.69
−0.19
ΔEP
0.31
0.62
ΔFG
0.71
ΔY
0.28
N$_{ut}$
0.66
N$_{up}$
−0.76
N$_{loss}$
Per-tiller N uptake (N$_{ut}$)
Soil N loss (N$_{loss}$)
Per-panicle N uptake (N$_{ut}$)
Effective panicles (EP)
Per-panicle filled grains (FG)
Shrunken and empty grains
Vegetative phase
Reproductive + Ripening phase

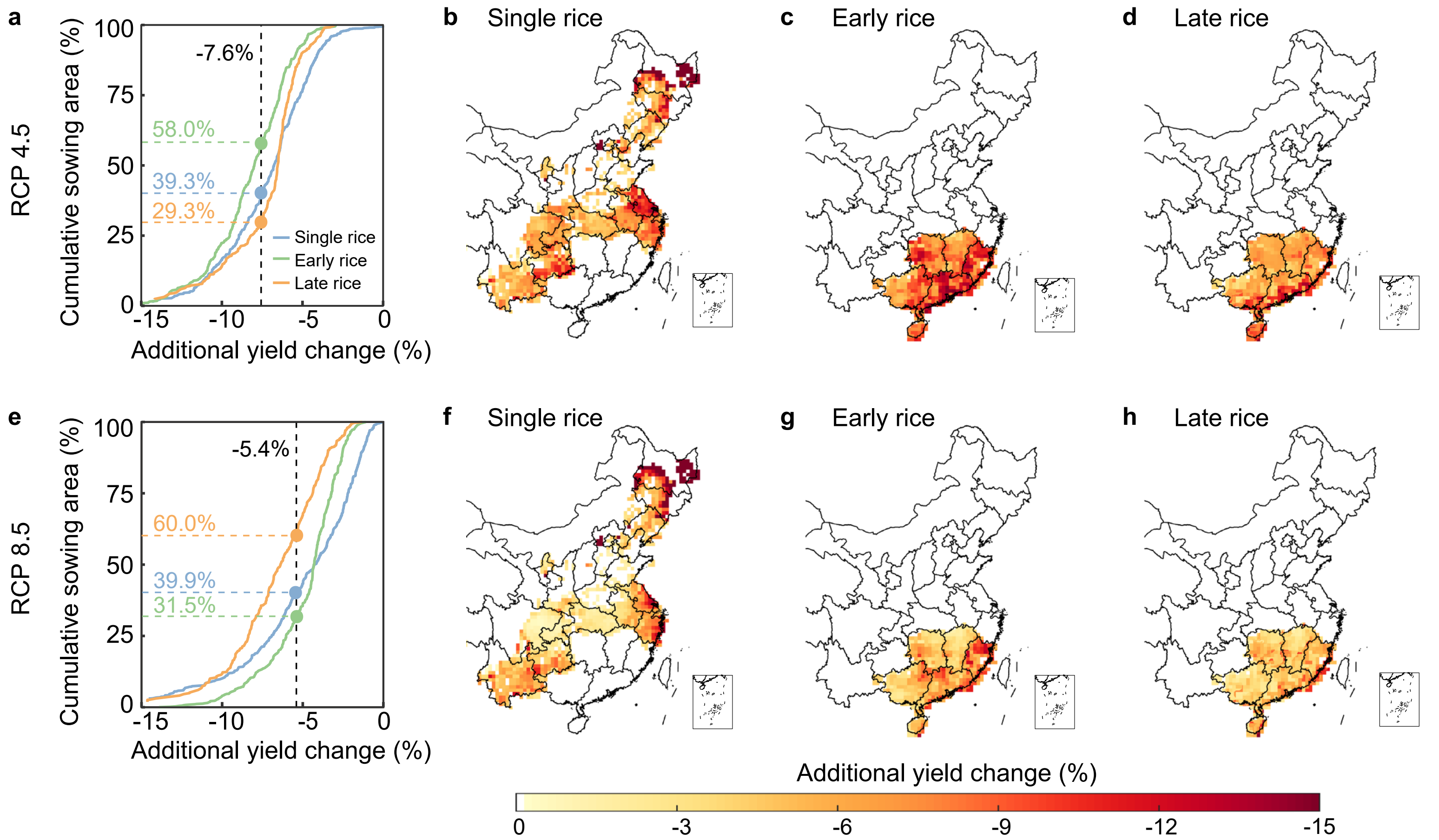
a
b Single rice
c Early rice
d Late rice
RCP 4.5
Cumulative sowing area (%)
-7.6%
58.0%
39.3%
29.3%
Single rice
Early rice
Late rice
Additional yield change (%)
e
f Single rice
g Early rice
h Late rice
RCP 8.5
-5.4%
60.0%
39.9%
31.5%
Additional yield change (%)
0
-3
-6
-9
-12
-15

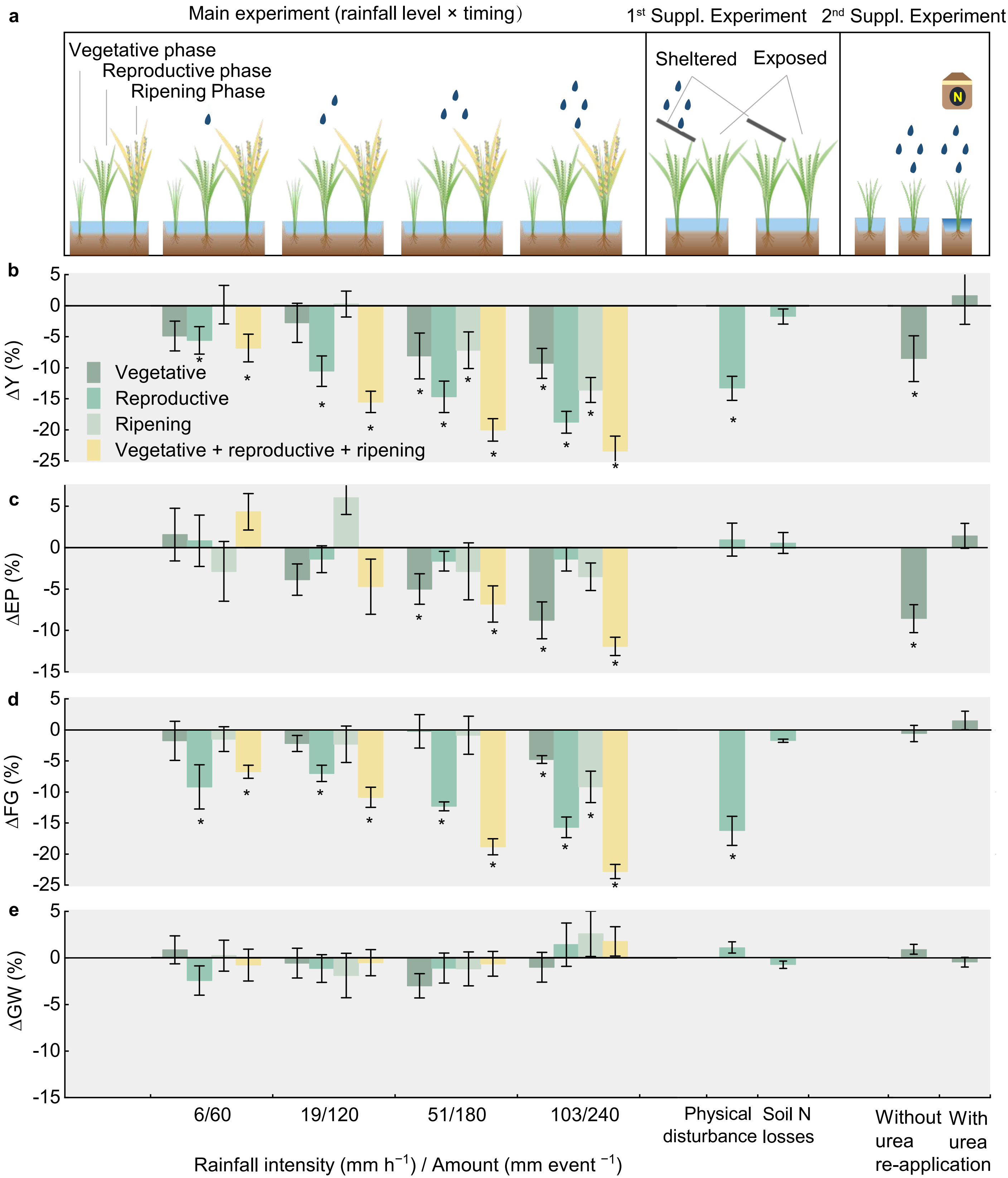
a
Main experiment (rainfall level × timing)
1st Suppl. Experiment
2nd Suppl. Experiment
Vegetative phase
Reproductive phase
Ripening Phase
Sheltered
Exposed
N
b
ΔY (%)
Vegetative
Reproductive
Ripening
Vegetative + reproductive + ripening
c
ΔEP (%)
d
ΔFG (%)
e
ΔGW (%)
6/60
19/120
51/180
103/240
Physical disturbance
Soil N losses
Without urea
With urea re-application
Rainfall intensity (mm h−1) / Amount (mm event −1)

Supplementary text

1. Quantification of ΔY induced by climate extreme events
2. Representativeness of observation dataset used for historical analysis

Supplementary Tables

1. Correlations between ΔY and extreme rainfall indices.
2. Model equations derived from the best-fit structural equation model.
3. Definition of climate extremes translated from the China meteorological administration.
4. Physicochemical properties of topsoil in the experimental site.
5. Model input data for historical simulations and future projections.

Supplementary Figures

1. Field observation network of rice yield, phenology, and extreme climate events during 1999-2012.
2. Comparison in the effects of different extreme events with similar percentiles.
3. Comparison of ΔY in response to extreme climate events of this study and three previous methods.
4. Frequency of individual yield responses to climate extremes.
5. Correlations between ΔY and extreme rainfall parameters.
6. Experimental evidence of the extreme rainfall-rice yield relationship.
7. Field setup of main experiment conducted from 2018 to 2019.
8. Field setup of the supplementary experiment conducted in 2021.
9. Differences in floret, grains, and grain distribution revealed by the first supplementary experiment.
10. Experimental relationships between soil N loss and changes in effective panicle.
11. Structural equation modeling for hypothesis tests.
12. Performance of the ORCHIDEE-Crop model with the extreme rainfall processes for simulating rice yields.
13. Regional assessments of rainfall-induced rice yield reductions in 2001-2016 based on the model with the extreme rainfall processes.
14. Relative change in extreme rainfall in 2085-2100 compared to that in 2001-2016 under RCP 4.5 and RCP 8.5.
15. Patterns of extreme rainfall across the Asian rice fields.
16. Probability distributions of extreme rainfall from three data sets during 2001-2016.
17. N application rates and rainfed ratios across the Asian rice fields.
18. Examples to identify the control-treatment pairs using a window searching strategy.
19. Comparison of yield observations and estimation from yield components.
20. Performance of the panel regression model to exclude the effects from inter-annual variations in climate conditions.
21. Comparison of ΔY in response to extreme rainfall using three window widths.
22. Nationwide observational stations within the rice production areas in China during 1999-2012.

Supplementary text 1. Quantification of ΔY induced by climate extreme events

We used a window searching strategy to quantify the change in rice yield (ΔY) induced by each extreme climate event. ΔY is defined as the relative change in rice yield between the treatment (YT) and control (YC) cases (in %), where the control-treatment pair was identified for the same site and rice type (Supplementary Fig. 18). The national agrometeorological observation network provided observations of rice yields and extreme climate events, offering the opportunity to identify the control-treatment pairs. As differences between control and treatment for each site and rice type are not only influenced by extreme climate events, but also by changes in rice cultivar and phenology and the interannual weather variability, we isolated ΔY induced by climate extremes by controlling for effects of cultivar, phenology and weather variability for each site and rice type as follow:

$$\Delta Y_{i,t,u,m} = \frac{\left(YT_{i,t,u,m}^{de} - YT_{i,t,u,m}^{fit}\right) - \left(\overline{YC}_{i,k,u,m}^{de} - \overline{YC}_{i,k,u,m}^{fit}\right)}{\overline{YC}_{i,k,u,m}^{de}} \times 100\%, \tag{1}$$

where *t*, *k*, *i*, *u*, and *m* refer to year of the treatment, year of the control, site, rice type, and event type, respectively. $YT_{i,t,u,m}^{de}$ and $YT_{i,t,u,m}^{fit}$ refer to the detrended yield and fitted yield in the treatment, respectively. $\overline{YC}_{i,k,u,m}^{de}$ and $\overline{YC}_{i,k,u,m}^{fit}$ refer to the mean rice yield in the control after being detrended and fitted, respectively, if identifying multiple controls within a 7-year window[1].

First, we detrend rice yield to exclude the effects from changes in rice cultivar and phenology for each site and rice type as follows:

$$Y_{i,t,u}^{de} = Y_{i,t,u} - (\alpha_{i,u} \times Year_t + \beta_{i,u}) + \bar{Y}_{i,u},\ \forall i,\ u, \tag{2}$$

where $Y_{i,t,u}$ and $Y_{i,t,u}^{de}$ refer to rice yield before and after being detrended, respectively, at site *i* of rice type *u* in year *t*. $\alpha_{i,u}$ and $\beta_{i,u}$ refer to coefficients of the temporal linear trend of the observed rice yield ($Y_{i,u}$) against observational years. $\bar{Y}_{i,u}$ refers to the mean of $Y_{i,u}$ at site *i* of rice type *u* during the observational year 1999-2012.

Second, we use a panel regression model to remove the effects from inter-annual variations in climate conditions, based on all observations without records of extreme climate events:

$$\begin{aligned} Y_{i,t,u}^{fit} = {} & \beta_1 Temp_{i,t,u} + \beta_2 Prec_{i,t,u} + \beta_3 Ssd_{i,t,u} + \beta_4 Temp_{i,t,u}^2 + \\ & \beta_5 Prec_{i,t,u}^2 + \beta_{6,i} Year_t + \beta_{7,i} Year_t^2 + Site_i + \varepsilon_{i,t,u}, \end{aligned} \tag{3}$$

where $Y_{i,t,u}^{fit}$ is the fitted yield at site *i* of rice type *u* in year *t*; β represents model parameters obtained from the regression of $Y_{i,u}^{de}$; ε is an error term; $\beta_{6,i}Year_t + \beta_{7,i}Year_t^2$ are the site-specific quadratic polynomials time trends; $Site_i$ corresponds to the time-invariant site-fixed effect to control for time-invariant heterogeneity. This model showed sufficient predictive capability, explaining 55% of rice yield variations (Supplementary Fig. 20).

Third, we apply a window searching strategy to identify all available control-treatment pairs, where in the treatment rice has been exposed to a given extreme event during the rice growing season, and in the control, rice has not been exposed to that event and other extreme events either did not occur or were the same as in the treatment. Both of the treatment and control for each pair are detected from the same site and rice type. All the available controls were identified within a 7-year moving window for each treatment. The controls were identified for ΔY only when at least one control is detected, otherwise the window moves to cover another 7-year observation of rice yield. YC were averaged if multiple controls were detected within a 7-year window. We elaborate the procedure for identifying control-treatment pairs in Supplementary Fig. 18. After that, we determine $YT_{i,t,u,m}^{de}$, $YT_{i,t,u,m}^{fit}$, $\overline{YC}_{i,k,u,m}^{de}$, and $\overline{YC}_{i,k,u,m}^{fit}$, and accordingly calculate ΔY based on the Equation 1. In addition, a sensitivity analysis was done to test if the quantification of ΔY depends on the range of moving windows — that is, 5 years and 9 years. The results indicate that the quantification of ΔY is insensitive to the choice of moving windows (Supplementary Fig. 21).

This strategy expands on previous studies[1-9] in at least three aspects: (i) It ensures both control and treatment sharing approximately the same management practices (e.g., fertilization, irrigation, and drainage) and geographical conditions (e.g., soil properties and topography), while almost avoiding technology- or cultivar-driven change in rice yield; (ii) it isolates the impact of a given extreme event on rice yield while largely reducing the noise due to the other events, and (iii) it provides an observational evidence for climate extreme impacts on rice yield at the site scale, rather than expected signal from statistical inferences at administrative scales.

Finally, we verify the robustness of ΔY by comparing the results from our window searching strategy with those from three previous methods (Supplementary Fig. 4). The analyses of previous methods are based on the observations of rice yield along with at least one record of extreme event over the period 1999-2012 (n = 1,826).

(i) Superposed epoch analysis[1]. We re-organized the yield data into two types of composited series, i.e., the treatment composited series (TS) and control composited series (CS). For each site and extreme climate event, we extracted short sets of time series of rice yield using a 7-year window, and centered the treatment, with 3 years of data preceding and following. Then, the yield data within 7-year window were normalized to the average of 3 years preceding and following. Yields were excluded from the mean when the occurrence of another extreme climate events in the TS, resulting in variable sample size across the 7 years of the composites. To set up CS, we first identified control by randomly resampling the rice yield data from site-years without any extreme climate event occurred. Then we normalized each control point the same as for the treatment, and the entire process was repeated 1,000 times. We quantified ΔY by subtracting the means of TS from the mean of CS. The results of the superposed epoch analysis showed that rice yield reduction induced by extreme rainfall (3.8±0.2%, n=135) was larger in relative to other extreme events, i.e., 2.8±0.2% for extreme heat (n=7), 0.7±0.4% for drought (n=79), 2.7±0.2% for extreme cold (n=118), and 1.0±0.2% for other extreme events (n=55). These yield reductions were generally lower than that obtained from the other methods, which could be attributed to the limited sample size for the super epoch analysis (Supplementary Fig. 4).

(ii) Time series analysis[3]. The impact of extreme climate events on crop yield for a given site can be quantified by comparing the crop yield in the treatment (YT) with that expected from its long-term yield trend (YT^{exp}). We calculate ΔY as the relative change in rice yield between YT and YT^{exp} (in %) as below:

$$\Delta Y_{i,t,u,m} = \frac{\left(YT_{i,t,u,m} - YT^{exp}_{i,t,u,m}\right)}{YT^{exp}_{i,t,u,m}} \times 100\%, \tag{4}$$

where $\Delta Y_{i,t,u,m}$ refers to rice yield change due to extreme climate type m at site t of rice type u in year i. It should be noted that this method might overestimate ΔY as for more than half of observations, multiple extreme events were coincided, and the effect of a given extreme event cannot be distinguished. Results showed that rice yield reduction induced by extreme rainfall (7.9±0.9%, n=217) was larger than drought (6.2±1.0%, n=152), extreme cold (5.3±0.8%, n=163) and other extreme events (4.9±1.1%, n=114), and not significantly different from extreme heat (7.1±1.7%, n=61).

(iii) Panel regression model[10]. We built a panel regression model to connect rice yield with climate variables ($Temp$, Ssd, extreme rainfall, drought, extreme heat and cold), edaphic properties (Clay content and SOC), agricultural management practices (irrigation and fertilizer application) as below:

$$\begin{gathered}\log\left(Y^{de}_{i,t,u}\right) = \alpha_1 Temp_{i,t,u} + \alpha_2 Ssd_{i,t,u} + \alpha_3 RX1h_{i,t,u} + \alpha_4 Rg1event_{i,t,u} + \\ \alpha_5 Drought_{i,t,u} + \alpha_6 Heat_{i,t,u} + \alpha_7 Cold_{i,t,u} + \alpha_8 Fert_{i,t,u} + \alpha_9 Irri_{i,t,u} + \\ \alpha_{10} Clay_{i,u} + \alpha_{11} SOC_{i,u} + Site_i + RiceT_u + \alpha_{12,i} Year_t + e_{i,t,u},\end{gathered} \tag{5}$$

where $Temp_{i,t,u}$ and $Ssd_{i,t,u}$ refer to mean daily temperature and total sunshine hours over rice growing season, respectively. $RX1h_{i,t,u}$ and $Rg1event_{i,t,u}$ are defined as the extreme rainfall intensity and its event amount, respectively. $Drought_{i,t,u}$ is defined as the minimum standardized precipitation evapotranspiration index over rice growing season. $Heat_{i,t,u}$ and $Cold_{i,t,u}$ are defined as the maximum and minimum hourly temperature over rice growing season, respectively. $Site_i$ and $RiceT_u$ correspond to the time-invariant fixed effect of site and rice type, respectively, to control for time-invariant heterogeneity. $\alpha_{12,i}Year_t$ correspond to linear site-specific time trends. It should be noted that total precipitation over the rice growing season was excluded because of the collinearity between total precipitation and extreme rainfall event amount. Coefficients $\alpha_1 \sim \alpha_{11}$ refer to sensitivities of yield to climatic, edaphic, and management-related variables. For instance, a unit increase in $Temp$ is associated with $\alpha_1 \times 100\%$ yield decline, and thus the ΔY induced by mean temperature increase is calculated as the increase in $Temp$ multiplied by $\alpha_1 \times 100\%$[10]. The panel regression model explained 58% of rice yield variations. Results showed that extreme rainfall induced rice yield decline of 5.0±0.3% (n = 217), which was comparable to drought (4.7±0.1%, n = 152), but higher than extreme heat (4.5±0.1%, n = 61) and extreme cold (2.1±0.02%, n = 163). Note that this model did not quantify the ΔY induced by the other extreme events (e.g. hail, typhoon and tropical cyclones).

Combining the results of three previous methods concluded that the yield reduction due to extreme rainfall (5.8±1.2%) was comparable to that due to extreme heat (4.8±1.3%), and larger than the reductions related to drought (3.9±1.7%), extreme cold (3.4±1.0%), and the other extreme events (2.9±1.6%). This finding was well consistent with that of our window searching strategy (Supplementary Fig. 4).

Supplementary text 2. Representativeness of observation dataset used for historical analysis

The national agrometeorological observation stations are by far limited and not homogeneously distributed over the rice production areas in China, resulting in a potential lack of representativeness. We cannot exclude the uncertainty of observation representativeness, but conduct an additional analysis to investigate how well our dataset can spread across the rice production areas in China. Following the approach of Beer et al.[11], we compared the distributions of climate indices (average and extreme) between the datasets from study stations in 1999-2012 and all stations across China's rice production areas in 1981-2012. First, to test the representations of background climate variation over space, we compared the distribution of mean daily temperature and total rainfall during rice growing season from study stations with that at all stations. Second, to test the representations of extreme rainfall variation over space, we compared the distribution of its intensity and event amount during rice growing season from study stations (that involved in the extreme rainfall induced ΔY analysis) with those at all stations. The intensity is defined as the maximum hourly precipitation when exceeding the threshold, and the event amount is defined as the precipitation amount averaged for extreme rainfall events that involve at least one extreme rainfall and for which the break duration between hourly precipitation does not exceed 6 hours. Third, to test the representations of rainfall variation over time, we compared the kernel probability density curves of total rainfall during rice growing season from study stations with that at all stations. Two indicators (Kullback–Leibler divergence[12] and Jensen-Shannon divergence[13]) were used for assessment of the representativeness. Climate datasets were acquired directly from the national agrometeorological observation stations, including 1,237 stations within rice production area in China in 1981-2012.

The results indicate that our dataset can adequately capture the spatiotemporal heterogeneity of climate conditions across rice production areas in China (Supplementary Fig. 22), with the Kullback–Leibler divergence (KL) ≤ 0.1 and the Jensen-Shannon divergence (JS) <0.03 for the comparisons of the background climate, KL<0.3 and JS<0.07 for extreme rainfall conditions, and KL$=0.001$ and JS<0.001 for the comparison of rainfall variation over time.

Supplementary Table 1 Correlations between ΔY and extreme rainfall indices. It includes intensity (RX1h, cm h^{-1}), total intensity (RX1hTOT, cm) and its proportion to growing-season total precipitation (R99pPROP, %), frequency in proportion to growing season length (R99p, %), event amount (Rg1event, cm $event^{-1}$). The thresholds were defined as the 95^{th}, 99^{th}, or 99.9^{th} percentiles of hourly precipitation during growing season in the reference period during 1981–2012 for each site. Extreme rainfall event was defined as events that involve at least one extreme rainfall and for which the break between hourly precipitation lies below 2, 6, 12, and 24 hours. Data is the correlation coefficients of ΔY to indices. *p<0.05; **p<0.01; ***p<0.001, and n.s. for not significant.

Break	Threshold	ΔY v.s. RX1h	ΔY v.s. RX1hTOT	ΔY v.s. R99pPROP	ΔY v.s. R99p	ΔY v.s. Rg1event
2h	95.0^{th}	−0.16 (*)	−0.11 (n.s.)	−0.01 (n.s.)	−0.05 (n.s.)	−0.37 (***)
	99.0^{th}	−0.20 (*)	−0.07 (n.s.)	−0.03 (n.s.)	−0.01 (n.s.)	−0.38 (***)
	99.9^{th}	−0.28 (n.s.)	−0.07 (n.s.)	−0.02 (n.s.)	0.07 (n.s.)	−0.43 (**)
6h	95.0^{th}	−0.11(n.s.)	−0.11 (n.s.)	−0.02 (n.s.)	−0.07 (n.s.)	−0.35 (***)
	99.0^{th}	−0.21 (**)	−0.10 (n.s.)	−0.06 (n.s.)	−0.02 (n.s.)	−0.41 (***)
	99.9^{th}	−0.29 (n.s.)	−0.05 (n.s.)	0.01 (n.s.)	0.10 (n.s.)	−0.45 (**)
12h	95.0^{th}	−0.11 (n.s.)	−0.13 (n.s.)	0.00 (n.s.)	−0.09 (n.s.)	−0.36 (***)
	99.0^{th}	−0.20 (*)	−0.08 (n.s.)	−0.02 (n.s.)	−0.01 (n.s.)	−0.35 (***)
	99.9^{th}	−0.29 (n.s.)	−0.06 (n.s.)	0.00 (n.s.)	0.10 (n.s.)	−0.44 (**)
24h	95.0^{th}	−0.11 (n.s.)	−0.16 (*)	−0.05 (n.s.)	−0.15 (*)	−0.35 (***)
	99.0^{th}	−0.17 (*)	−0.08 (n.s.)	−0.02 (n.s.)	−0.02 (n.s.)	−0.33 (***)
	99.9^{th}	−0.31 (n.s.)	−0.07 (n.s.)	0.01 (n.s.)	0.10 (n.s.)	−0.17 (n.s.)

Supplementary Table 2 Model equations derived from the best-fit structural equation model

Equation	Description*
Change in effective panicle per unit land area (ΔEP)	
$\Delta EP = a_1 \cdot \Delta N_{ut} + b_1$	ΔEP: relative change in effective panicle during vegetative phase (%), ΔN_{ut}: relative change in N uptake per tiller of rice during vegetative phase (%), $a_1 = 0.262$, $b_1 = -1.644$.
$\Delta N_{ut} = a_2 \cdot \Delta N_{loss} + b_2$	ΔN_{ut}: relative change in N uptake per tiller during vegetative phase (%), ΔN_{loss}: change in N loss during vegetative phase induced by extreme rainfall (kg N ha^{-1}), $a_2 = -1.026$ and $b_2 = 7.054$.
$\Delta N_{loss} = (N_{l1} + N_{r1}) - (N_{l0} + N_{r0})$ for model performance assessment	ΔN_{loss}: soil N loss (kg N ha^{-1}), N_l: change in N loss via leaching (kg N ha^{-1}), N_r: change in N loss via runoff (kg N ha^{-1}), with the subscript 1 for extreme rainfall treatment and 0 for control.
$N_l = \left(0.0463 + 0.0037 \cdot \frac{P}{C \cdot L}\right) \cdot (F + \gamma \cdot D - U)$ for historical simulations and future projections	P: precipitation during the vegetative phase (mm), C: clay content (%), L: layer thickness or rooting depth (m), F: mineral and manure fertilizer N (kg N ha^{-1} yr^{-1}), γ: the decomposition rate of manure matter (% yr^{-1}), D: soil N density (kg N ha^{-1}), U: N uptake by crop (kg N ha^{-1}), according to ref.[14].
$N_r = EFP \cdot C_r + H_w \cdot (C_p - C_r) \cdot (1 - e^{-\frac{EFP}{H_r}}) + 2.2 \cdot C_p \cdot W \cdot T$ for historical simulations and future projections	EFP: effective precipitation per event during the vegetative phase, defined as the difference between precipitation and the sum of canopy interception and subsurface water fluxes (mm event^{-1}), C_r: mean N concentration of rainfall (mg L^{-1}), C_p : mean N concentration of ponded water (mg L^{-1}), H_w: mean ponded water level (mm), H_r: weir outlet height (mm), W: soil-water exchange velocity (cm s^{-1}), T: rainfall duration (s), according to ref.[15].
Change in filled grains per panicle (ΔFG)	
$\Delta FG = c \cdot KE_{re} + d \cdot KE_{ri} + e \cdot \Delta N_{up} + f$	ΔFG: relative change in filled grain, KE_{re}: time-specific kinetic energy during reproductive phase (J m^{-2} h^{-1}), KE_{ri} : time-specific kinetic energy during ripening phase (J m^{-2} h^{-1}), ΔN_{up}: relative change in N uptake per panicle due to the change in ΔN_{ut}, $c = -0.00424$, $d = -0.00115$, $e = 0.139$, $f = -3.676$.
$\Delta N_{up} = a_3 \cdot \Delta N_{ut} + b_3$	This correlation is confirmed by previous work[16], $a_3 = 0.723$, $b_3 = 1.592$.
$KE = 1288.17 \cdot \mu^{-1.34} \cdot Int^{(1+1.34 \cdot \beta)}$	Int: actual rainfall intensity ($mm\ h^{-1}$), following Salles et al.[17]. Constants that are linked to the type of microphysical process dominant in the raindrop growth. Since stratiform rain dominates in summer East Asia[18], we use constants corresponding to stratiform rain ($\mu = 40$ and $\beta = 0.21$) in this study.
$Int = \begin{cases} 0.736 \cdot D^{4.525}, & for\ D < 2.531mm \\ 10^{1.019 \cdot D - 0.891}, & for\ D \geq 2.531\ mm \end{cases}$	D: diameter of raindrop (mm), its correlation with *Int* is according to Nanko et al.[19].

Supplementary Table 3 Definition of climate extremes translated from the China meteorological administration

Event	Definitions*	References in Chinese
Extreme heat	A period of abnormally hot weather, if the daily maximum temperature exceeds 35°C.	http://zwgk.cma.gov.cn/zfxxgk/gknr/flfgbz/bz/202107/t20210716_3540198.html
Extreme cold	A period of abnormally cold weather, if daily mean temperature lies below that over the same period in history by one standard deviation.	http://zwgk.cma.gov.cn/zfxxgk/gknr/flfgbz/bz/202102/t20210210_2720477.html
Extreme rainfall	Intense rainfall with short duration, if daily precipitation exceeds 50 mm for rice planting regions in China where mean annual precipitation >400 mm.	http://zwgk.cma.gov.cn/zfxxgk/gknr/flfgbz/bz/202102/t20210210_2720509.html
Drought	A period of unusually low precipitation that produces a shortage of water for plants. It can be defined by different indices, such as standard precipitation index, standardized precipitation evapotranspiration index, and Palmer Drought Severity Index.	http://zwgk.cma.gov.cn/zfxxgk/gknr/flfgbz/bz/202102/t20210210_2719989.html
The other events	It included hail, wind, typhoon and tropical cyclone. A hail storm is a type of storm that is characterized by hail as the dominant part of its precipitation. The size of the hailstones can vary between pea size (6 mm) and softball size (112 mm) and therefore cause considerable damage. Wind is difference in air pressure resulting in the horizontal motion of air. The greater the difference in pressure, the stronger the wind. Wind moves from high pressure toward low pressure. A tropical storm originates over tropical or subtropical waters. It is characterized by a warm-core, non-frontal synoptic-scale cyclone with a low-pressure center, spiral rain bands and strong winds. Depending on their location, tropical cyclones are referred to as hurricanes (Atlantic, Northeast Pacific), typhoons (Northwest Pacific), or cyclones (South Pacific and Indian Ocean).	https://www.docin.com/p-2440560243.html http://zwgk.cma.gov.cn/zfxxgk/gknr/flfgbz/bz/202112/t20211221_4317166.html http://zwgk.cma.gov.cn/zfxxgk/gknr/flfgbz/bz/202102/t20210210_2720508.html

* These definitions are similar with the Emergency Events Database (EM-DAT) at https://www.emdat.be/Glossary.

Supplementary Table 4 Physicochemical properties of topsoil in the experimental site

Soil depth	0-20 cm	20-40 cm	40-60 cm	60-80 cm	80-100 cm
SOM	20.4	11.6	7.4	6.4	6.3
STN	1.2	0.8	0.6	0.5	0.6
STP	0.8	0.8	0.7	0.8	0.7
NH_4-N	2.4	1.9	1.7	1.8	1.5
NO_3-N	8.6	8.2	6.6	5.4	4.1
Olsen-P	29.4	22.2	14.4	31.8	15.0
Sand	0.4	0.6	0.4	0.7	0.2
Silt	79.8	82.2	81.8	80.3	76.5
Clay	19.8	17.2	17.8	19	23.3

The table depicts soil organic matter (SOM), soil total nitrogen (STN) and soil total phosphorus (STP) in g kg^{-1}, soil ammonium nitrogen (NH_4-N), soil nitrate nitrogen (NO_3-N), and soil available phosphorus (Olsen-P) in mg kg^{-1}, as well as soil texture including sand, silt and clay content in %.

Supplementary Table 5 Model input data for historical simulations and future projections

Input data	**Temporal resolution**	**Spatial resolution**	**Data source**	**Ref.**
Historical simulations				
Climate forcing*	Daily	0.5°	CRU-NCEP v8	[20]
Atmospheric CO_2 concentration	Annual	--	Ed Dlugokencky and Pieter Tans, NOAA/GML	[21]
Extreme rainfall intensity and event amount	Half hourly	0.1°	GPM (IMERG), version 6.0	[22]
Transplanting date	Fixed value	0.1° (interpolated from site-level observations)	National agrometeorological observation network	[23]
N loss via runoff	Event-based	0.1°	Calculated based on Table S4	[15]
N loss via leaching	Seasonal	0.1°	Calculated based on Table S4	[14]
N application rate	Seasonal	1km		[24]
Rice sowing area	Fixed value	1km		[24]
Future projections				
Climate forcing*	Daily	0.5°	IPSL earth system model	[25]
Atmospheric CO_2 concentration (RCP4.5, RCP8.5)	Annual	--		[26]
Extreme rainfall intensity and event amount	Half hourly	0.5°	IPSL earth system model	[25]
Transplanting date	Fixed value	0.1° (interpolated from site-level observations)	National agrometeorological observation network (consistent with historical simulation)	[23]
N loss via runoff	Event-based	0.1°	Calculated based on Table S4	[15]
N loss via leaching	Seasonal	0.1°	Calculated based on Table S4	[14]
N application rate	Seasonal	1km	Same as historical simulations	[24]
Rice sowing area	Fixed value	1km	Same as historical simulations	[24]

* It includes daily maximum temperature, daily minimum temperature, precipitation rate, surface wind, near-surface air temperature, surface air pressure, air specific humidity, surface downwelling, shortwave radiation, surface downwelling, and longwave radiation.

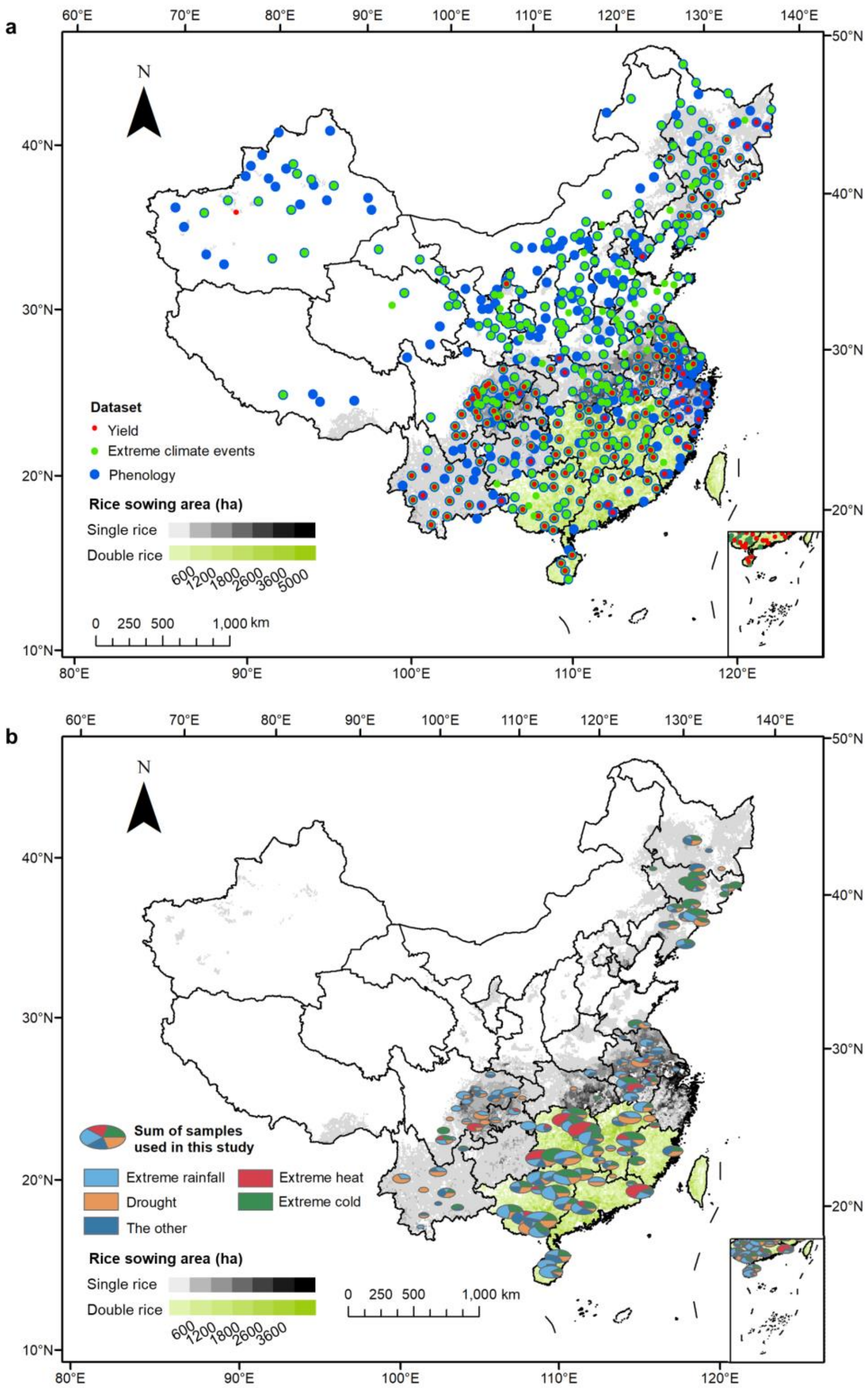

Supplementary Fig. 1 Field observation network of rice yield, phenology, and extreme climate events during 1999-2012. Note that panel **b** shows the distribution of the 707 control-treatment pairs filtered by a window searching strategy. The map was generated in MATLAB R2020a (MATLAB and Statistics Toolbox Release R2020a, The MathWorks). The base map of the country boundaries was from the Global Administrative Areas dataset (https://gadm.org).

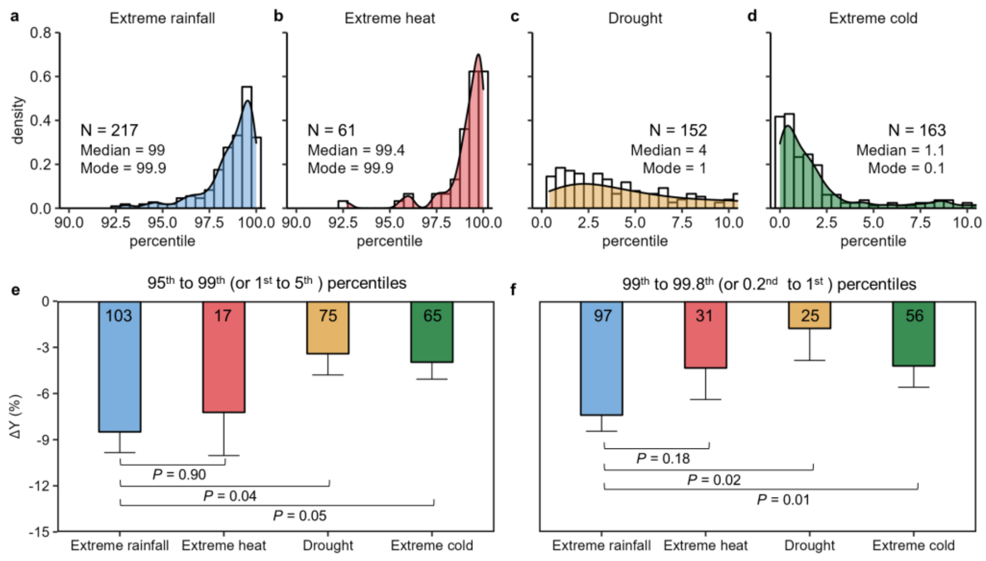

Supplementary Fig. 2 Comparison in the effects of different extreme events with similar percentiles. a. Histogram with kernel density estimation (hereinafter referred to as histogram) of extreme rainfall based on data of the maximum hourly precipitation recorded in given days for different sites and treatment years, **b**. Histogram of extreme heat based on data of maximum hourly air temperature recorded in given days for different sites and treatment years, **c**. Histogram of drought based on data of the minimum standardized precipitation evapotranspiration index[27] recorded in given days for different sites and treatment years, **d**. Histogram of extreme cold based on data of the minimum hourly air temperature recorded in given days for different sites and treatment years, **e**. Comparison of effects of extreme events with the similar percentiles from 95th to 99th for extreme heat and rainfall and from 1st to 5th for extreme cold and drought, **f**. Comparison of effects of extreme events with the similar percentiles from 99th to 99.8th for extreme heat and rainfall and from 0.2nd to 1st for extreme cold and drought. For panels **e** and **f**, data are presented as mean ± standard error. Numbers on the column refer to the sample size. Statistical significance of the differences in mean ΔY between extreme rainfall and other events are based on two-sided bootstrap t-test. For each of the 707 control-treatment pairs, we calculated the percentile of climate extremes recorded in year of the treatment relative to the base period 1981–2012. The data used was from the site observations run by the China Meteorological Administration (CMA). Both median and mode values were estimated.

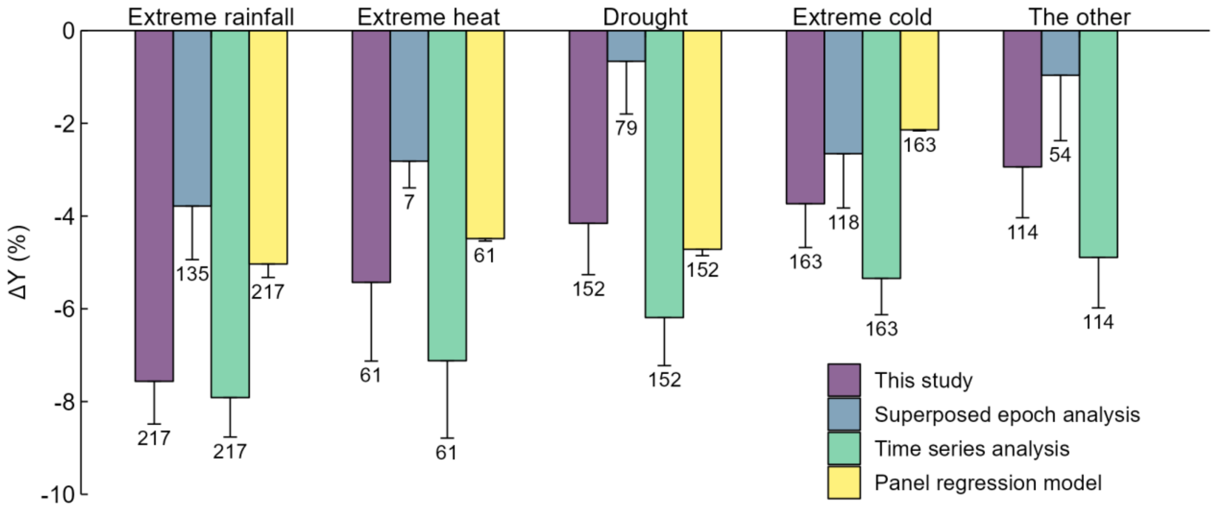

Supplementary Fig. 3 Comparison of ΔY in response to extreme climate events of this study and three previous methods. Columns are shown as mean and one standard error that were derived from this study and the other three methods: superposed epoch analysis[1], time series analysis[3], and a panel regression model[10]. Data are presented as mean ± standard error. Numbers on the column refer to the sample size. The significance between this study and the mean of other methods were tested using two-sided Paired Samples Wilcoxon Signed Rank Test with α=0.05.

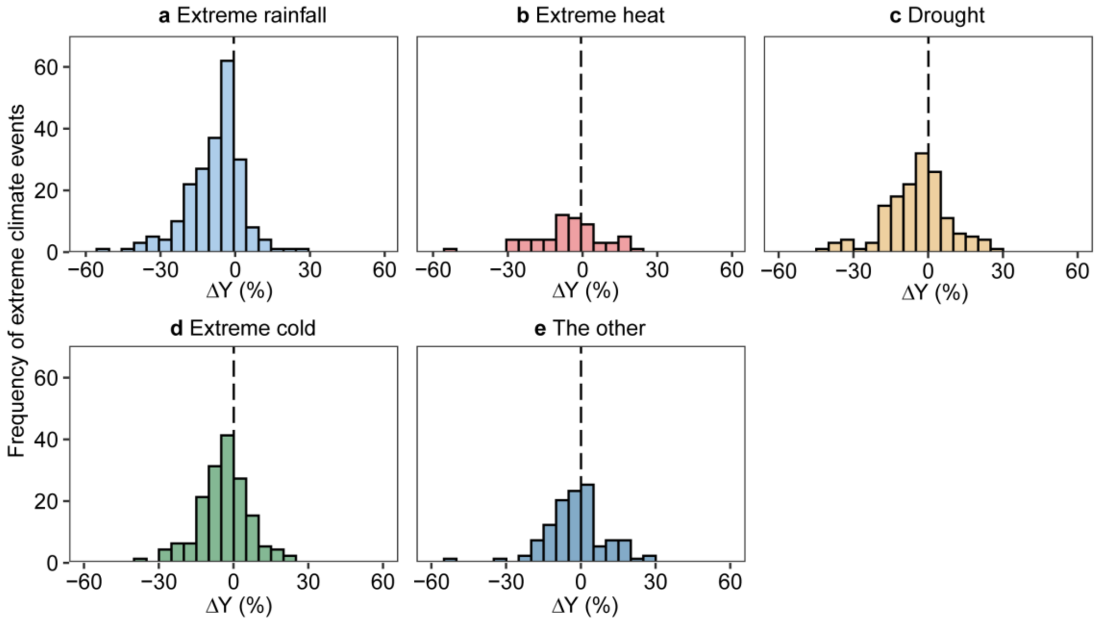

Supplementary Fig. 4 Frequency of individual yield responses to climate extremes. a. ΔY due to extreme rainfall, **b**. ΔY due to extreme heat, **c**. ΔY due to drought, **d**. ΔY due to extreme cold, **e**. ΔY due to the other events (typhoon and tropical cyclones). A preponderance of moderately negative values (falling towards the left areas of the dashed lines) underlies the negative mean climate extreme response signals, with a limited influence of a few outliers (those at the right areas of the dashed lines).

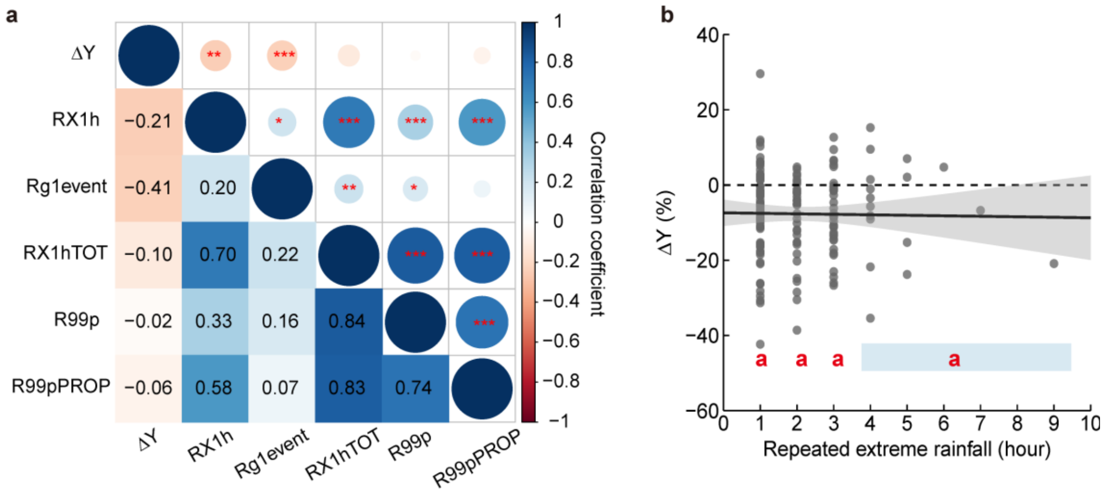

Supplementary Fig. 5 Correlations between ΔY and extreme rainfall parameters. a. Univariate Pearson's correlation coefficients for the effects of seven extreme rainfall parameters on ΔY (n=154): RX1h refers to the maximum hourly precipitation exceeding the threshold (cm h^{-1}); Rg1event refers to event amount that is the precipitation amount averaged for extreme rainfall events (cm per event); RX1hTOT refers to total intensity that is the sum of hourly precipitation when exceeding the threshold (cm); R99p refers to frequency that is the fraction of the hours when hourly precipitation exceeds the threshold divided by the length of rice growing season in hours (%); R99pPROP refers to proportion that is the sum of hourly precipitation exceeding the threshold divided by the growing-season total precipitation (%). Numbers and colors indicate for correlation coefficients, with *$p<0.05$; **$p<0.01$; ***$p<0.001$. **b.** The relationship between ΔY and repeated extreme rainfall defined as hours when hourly precipitation exceeds the threshold during rice growing season. The Kruskal-Wallis Rank Sum Test and Dunn's test were used for testing significance among hours of repeated extreme rainfall, since it's neither conform to a normal distribution (Shapiro-Wilk test, $p<0.001$) nor meet the homogeneity of variances (Bartlett's test, $p=0.001$). Blue shadows in panel **b** covered frequency≥4, with the same letters indicating for not significant differences in comparison with other frequencies, $\alpha=0.05$. Threshold of extreme hourly rainfall was defined as the 99th percentile. Rainfall event was defined with the break between rainfall no more than 6 hours.

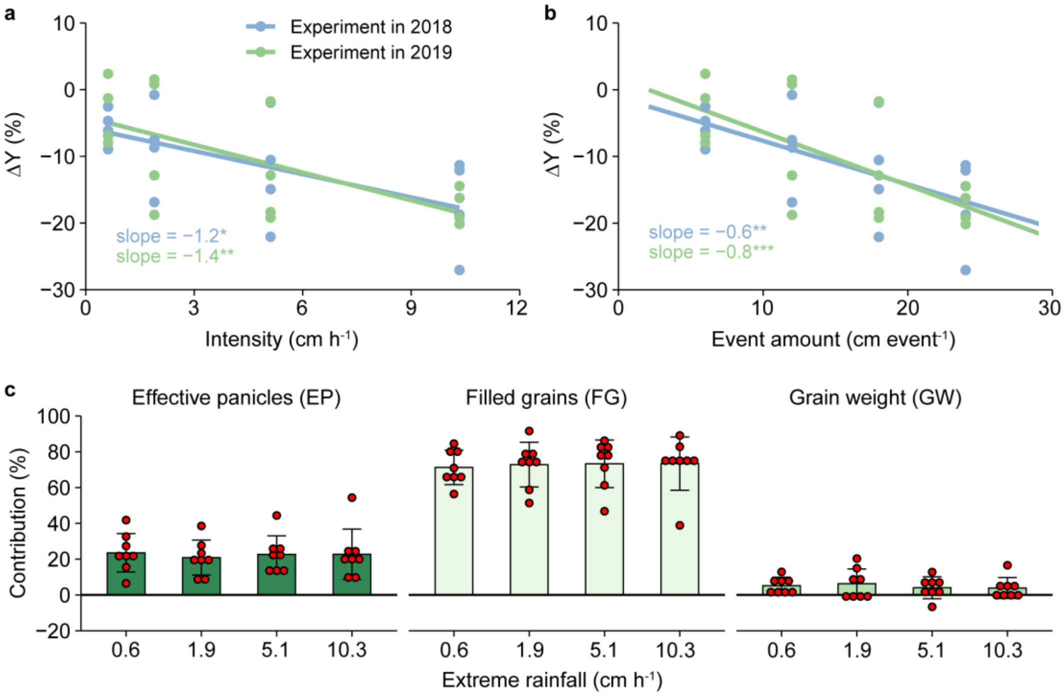

Supplementary Fig. 6 Experimental evidence of the extreme rainfall-rice yield relationship. a. ΔY v.s. extreme rainfall intensity. **b**. ΔY v.s. extreme rainfall event amount; for panels **a** and **b**, no significant differences were found between two experiment years, with n = 16 for each year. The solid line is the best-fit line, with *p<0.05; **p<0.01; ***p<0.001. **c**. Attribution of relative changes in effective panicle per unit land area (ΔEP), filled grains per panicle (ΔFG), and grain weight (ΔGW) to ΔY, following the Kaya identity approach[28], that is ΔY = ΔEP + ΔFG + ΔGW. Data are presented as mean ± standard error, with n = 8 for each intensity.

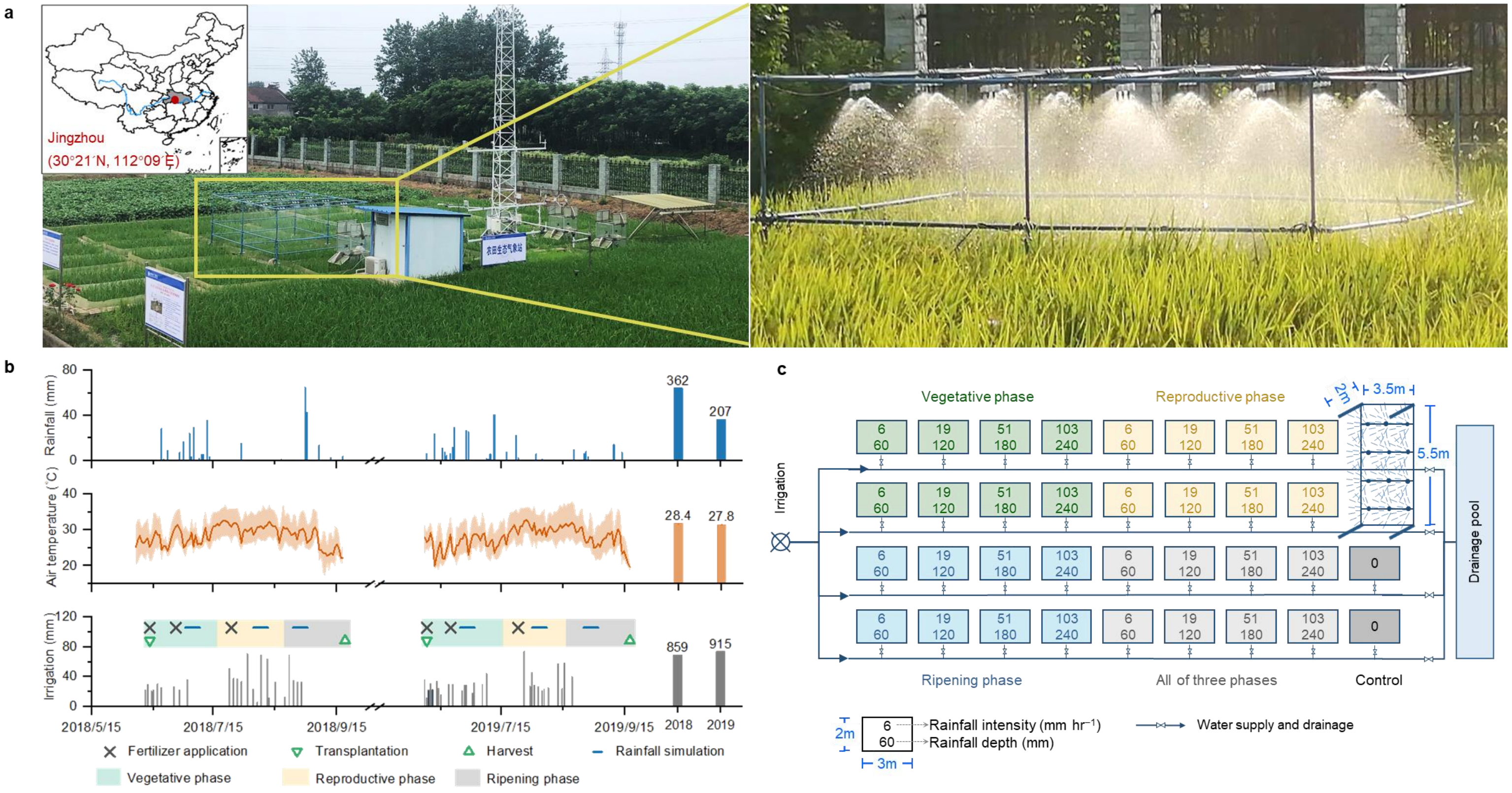

Supplementary Fig. 7 Field setup of main experiment conducted from 2018 to 2019. a. Field location and the artificial rainfall simulation system. **b**. Climate, fertilization, and irrigation conditions. **c**. Schematic diagram of field layouts and rainfall manipulations. Rainfall manipulations were conducted in 3rd July - 6th July in vegetative phase, 6th August - 9th August in reproductive phase, and 26th August - 29th August in ripening phase of 2018, and in 27th June - 30th June in vegetative phase, 2nd August - 5th August in reproductive phase, and 28th August -31st August in ripening phase of 2019. Filled colors of panel **c** correspond to the manipulations conducted in different growth phases. Fertilizers of 172 kg N ha^{-1}, 61 kg P ha^{-1}, and 49 kg K ha^{-1} were applied over three events. The first one was 72 kg ha^{-1} N, 53 kg ha^{-1} P and 42 kg ha^{-1} K applied first day before rice transplanting, followed by 78.7 kg ha^{-1} N applied two weeks after transplantation and 20.9 kg ha^{-1} N, 8 kg ha^{-1} P and 7 kg ha^{-1} K applied during the jointing stage.

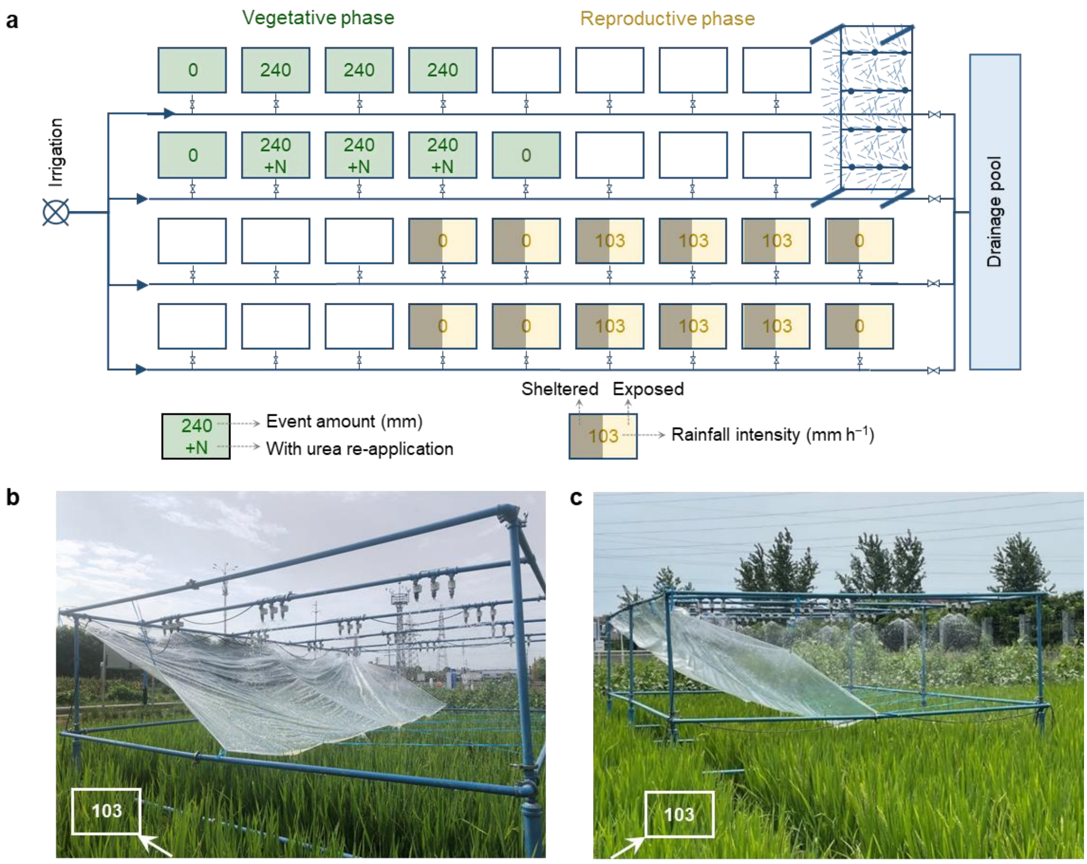

Supplementary Fig. 8 Field setup of the supplementary experiment conducted in 2021. a. Field layout of two supplementary experiments, with n = 3. **b** to **c**. Artificial rainfall simulation system with transparent rain shelter during reproductive phase, with the views from the right and left corners, respectively.

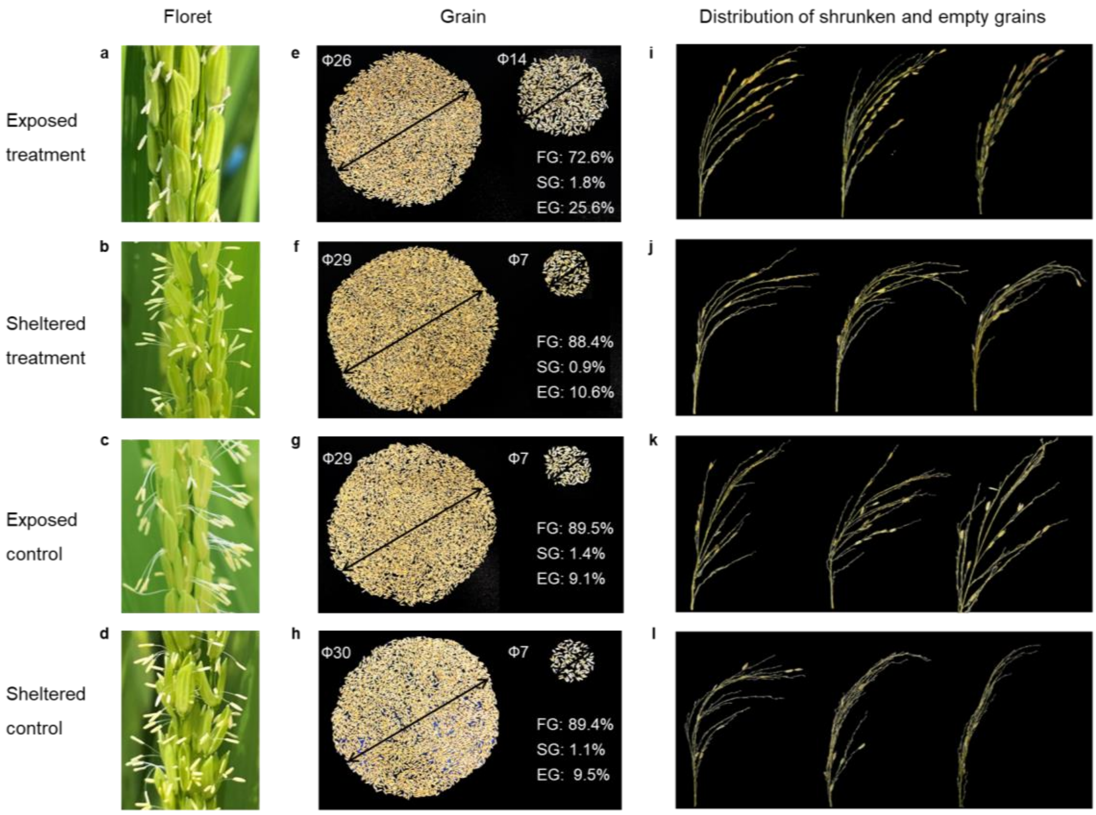

Supplementary Fig. 9 Differences in floret, grains, and grain distribution revealed by the first supplementary experiment. Panels **a** to **d** indicate that florets adhered to the surface of spikelet due to rainfall, while keeping normal for sheltered treatments and the controls. Panels **e** to **h** indicate that rainfall induced less filled grains (FG) but more empty or shrunken grains (EG or SG) than the sheltered treatments and the controls, based on 6 panicles randomly selected. Panels **i** to **l** indicate that empty or shrunken grains were found mainly in the upper part of the panicles for the exposed treatments, while in general distributing evenly along the panicles for the sheltered treatments and the controls, based on 3 typical panicles.

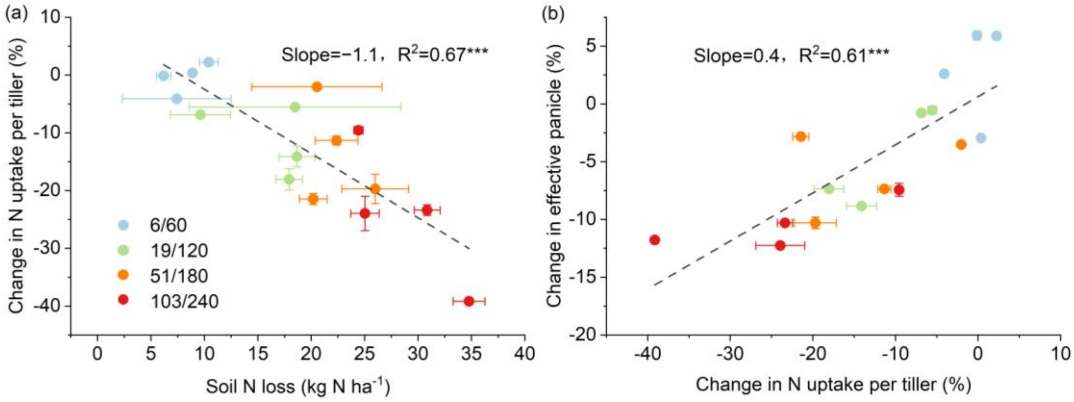

Supplementary Fig. 10 Experimental relationships between soil N loss and changes in effective panicle. a. Soil N loss v.s. Change in N uptake per tiller, **b**. Change in N uptake per tiller v.s. Change in effective panicle. Data are presented as mean ± standard error, with n = 4. In the legend, numbers before the slash indicate extreme rainfall intensity (mm h^{-1}), and numbers after indicate event amount (mm event^{-1}). The dash line is the best-fit line, with ***$p<0.001$.

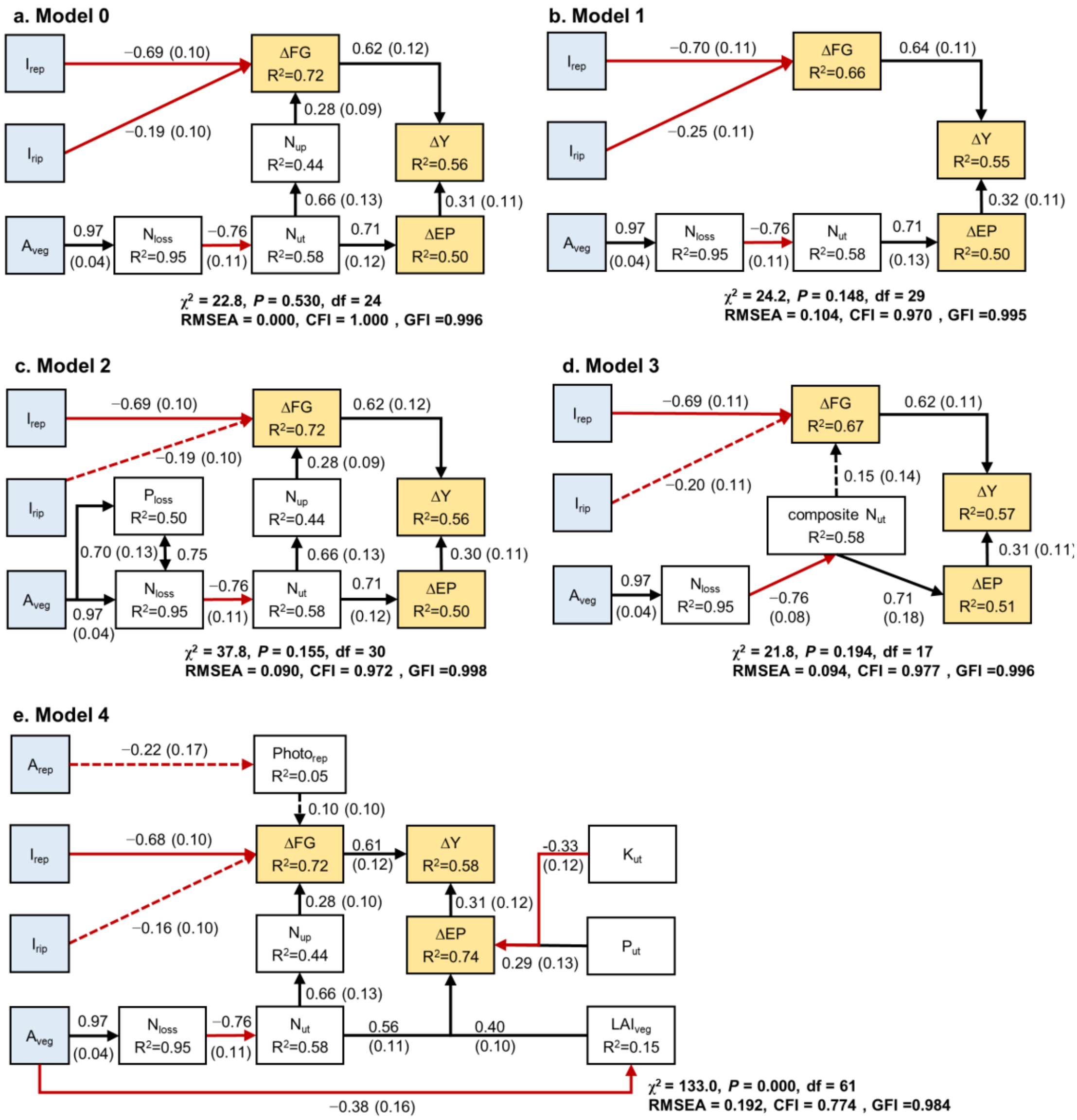

Supplementary Fig. 11 Structural equation modeling for hypothesis tests. A_{veg}, extreme rainfall event amount in vegetative phase; I_{rep} and I_{rip}, extreme rainfall intensity in reproductive and ripening phases, respectively; ΔY, ΔEP, and ΔFG, relative changes in rice yield, effective panicle, and filled grains, respectively; N_{loss}, N_{ut}, and N_{up}, relative changes in soil N loss, per-tiller N uptake during vegetative phase and per-panicle N uptake during reproductive phase, respectively; P_{loss}, P_{ut}, K_{ut}, relative changes in soil P loss, per-tiller P uptake, and per-tiller K uptake during vegetative phase, respectively; $Photo_{rep}$, photosynthetic rate in reproductive phase after rainfall manipulation; LAI_{veg}, leaf area index in vegetative phase. Solid black (red) arrows (with standardized path coefficients and standard errors in the brackets) indicate significant positive (negative) effects ($P < 0.05$), while dotted lines for insignificant effects. Data are averages for two replicates with n = 32.

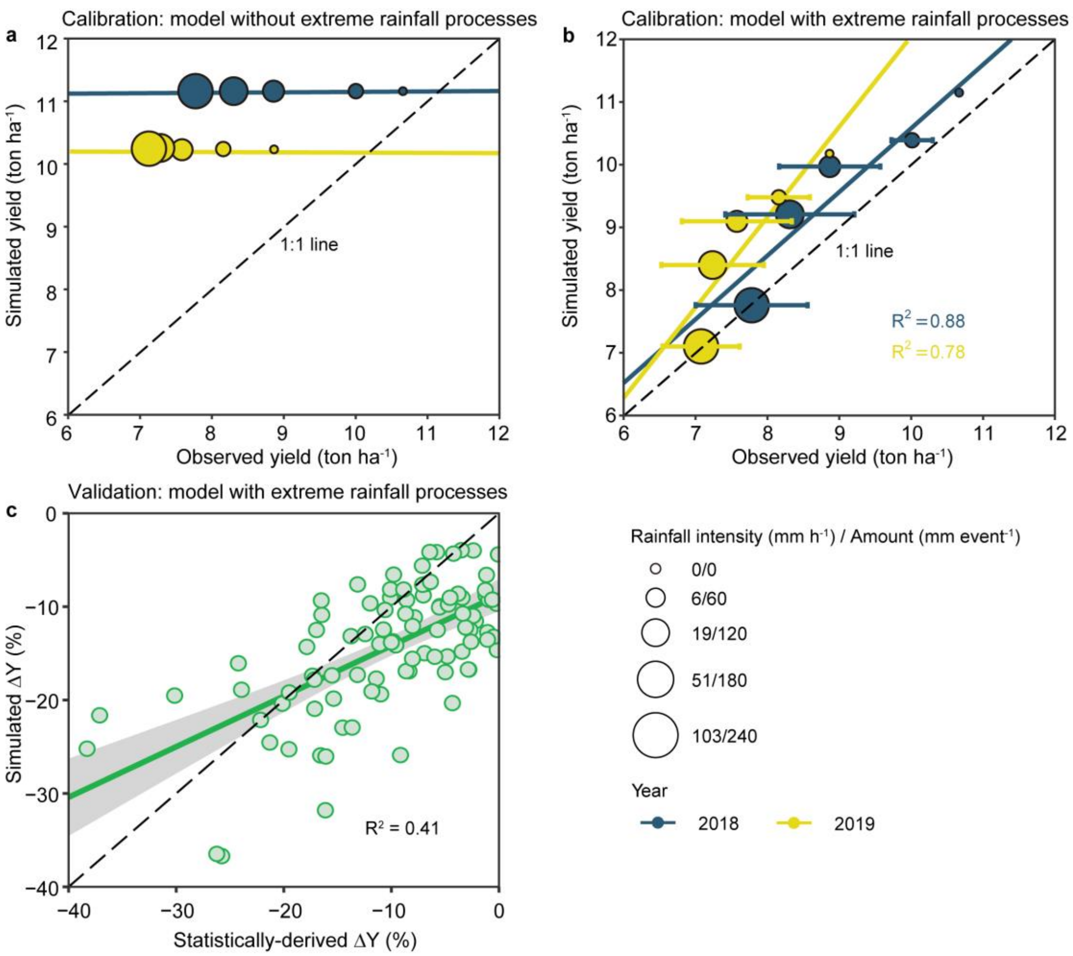

Supplementary Fig. 12 Performance of the ORCHIDEE-Crop model with the extreme rainfall processes for simulating rice yields. a-b Model calibration without and with extreme rainfall processes. The observed yield is obtained from the main experiment in 2018 and 2019. Dot size refers to rainfall levels, while colors for different experiment years. Data in panel **b** is shown as mean ± standard deviation. **c**. Model validation (n=95). We selected the observations with negative statistically-derived ΔY induced by extreme rainfall from the nationwide agrometeorological stations in 1999-2012, and local meteorology was used to force the model at each site. R^2 refers to coefficient of determination.

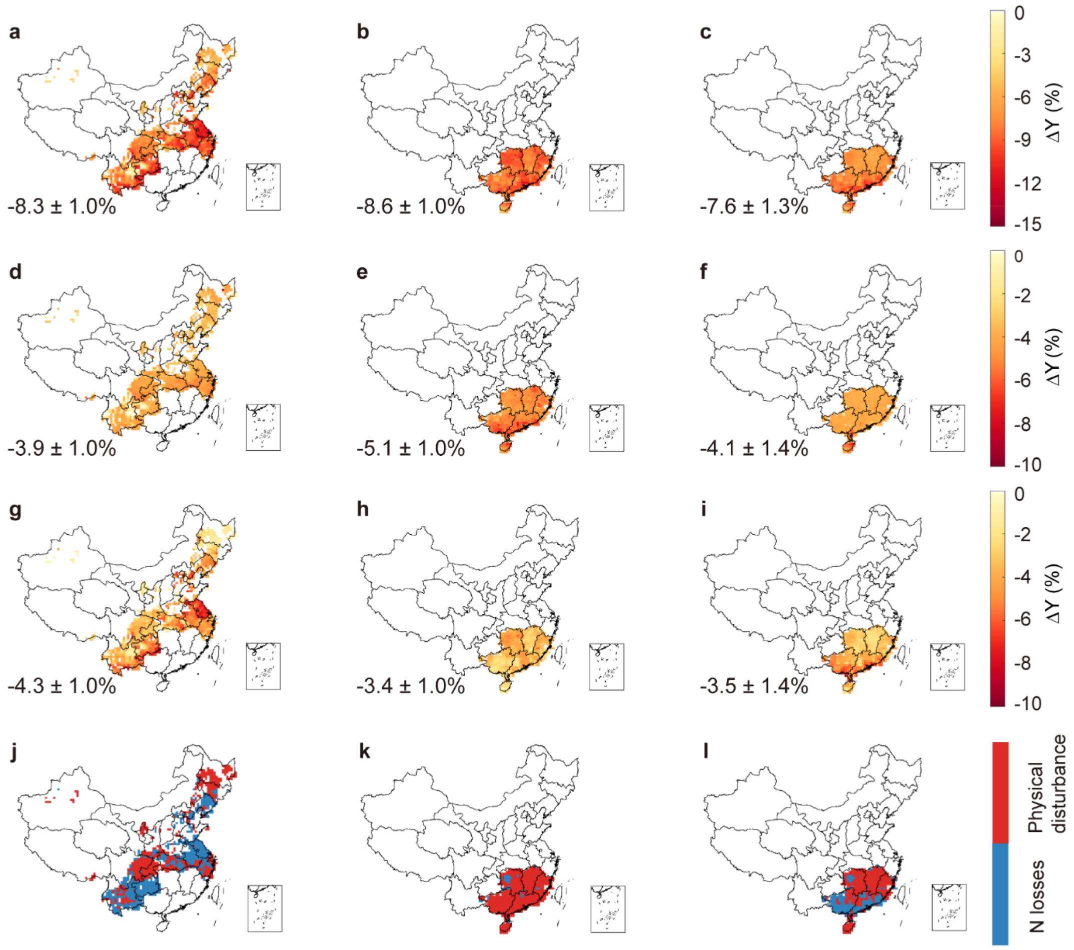

Supplementary Fig. 13 Regional assessments of rainfall-induced rice yield reductions in 2001-2016 based on the model with the extreme rainfall processes. a-c. Effects of rainfall-induced physical disturbance and N losses; **d-f.** Effects of rainfall-induced physical disturbance; **g-i.** Effects of rainfall-induced N losses. **j-l.** Dominant pathways of extreme rainfall impacts on rice yield. Left column is for single rice, middle column early rice, and right column late rice. The number in each panel indicates national mean relative change in rice yield weighted by sowing area and its standard error for interannual variability. The map was generated in MATLAB R2020a (MATLAB and Statistics Toolbox Release R2020a, The MathWorks). The base map of the country boundaries was from the Global Administrative Areas dataset (https://gadm.org).

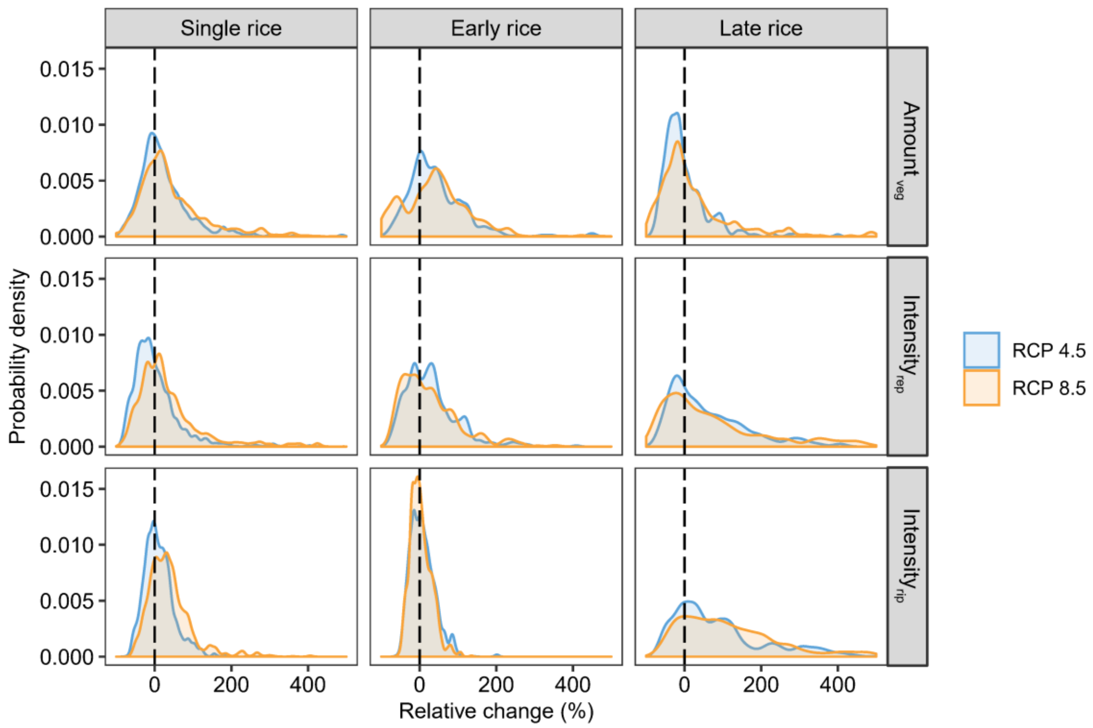

Supplementary Fig. 14 Relative change in extreme rainfall in 2085-2100 compared to that in 2001-2016 under RCP 4.5 and RCP 8.5. The relative change is calculated as the difference between IPSL-projected and IPSL-simulated extreme rainfall indices, including extreme rainfall event amount in vegetative phase ($Amount_{veg}$), extreme rainfall intensities in reproductive phase ($Intensity_{rep}$) and in ripening phase ($Intensity_{rip}$).

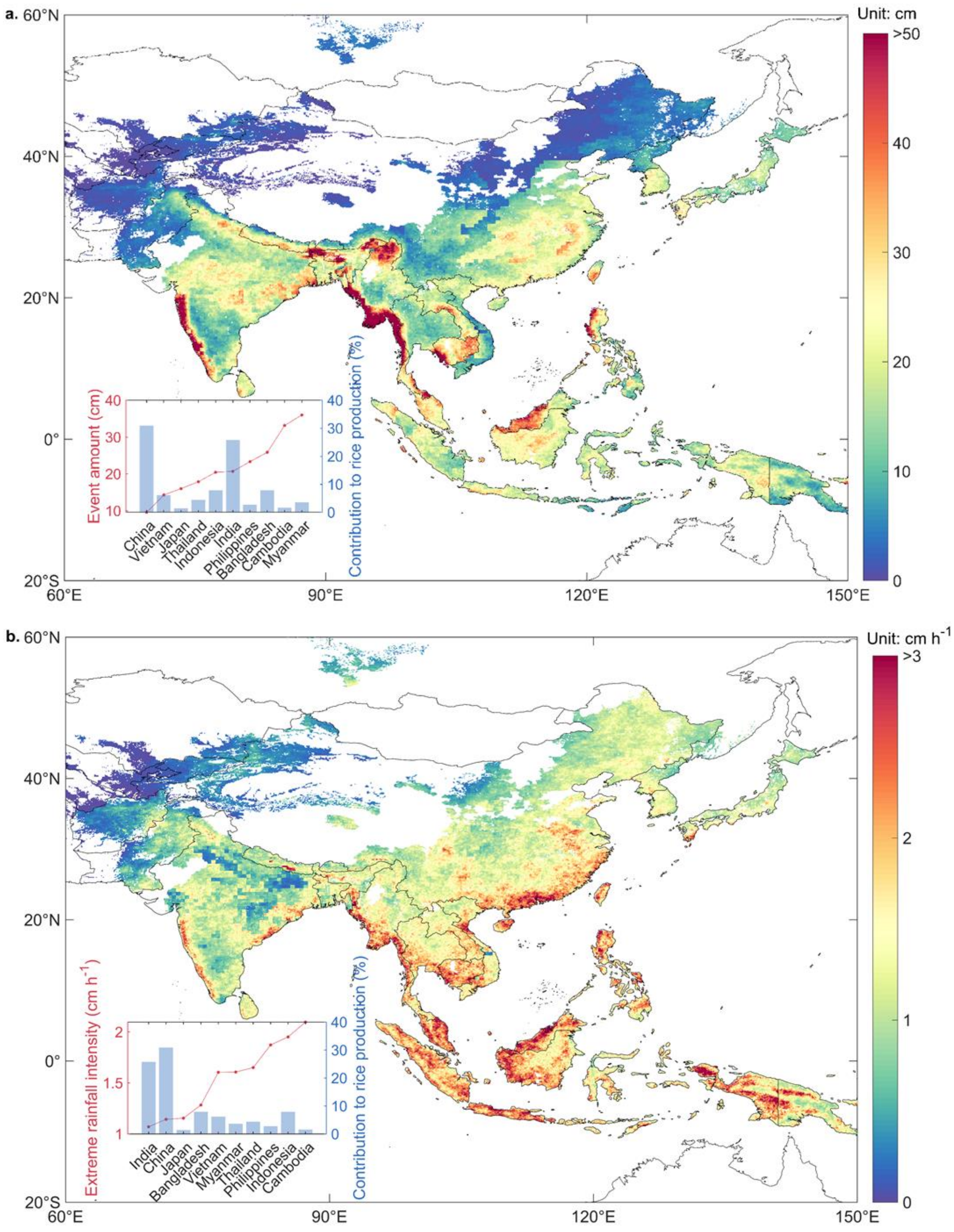

Supplementary Fig. 15 Patterns of extreme rainfall across the Asian rice fields. a. Cumulative extreme rainfall event amounts during vegetative phase averaged over the period 2001-2016, **b.** Extreme rainfall intensity during reproductive phase averaged over the period 2001-2016. The definitions of extreme rainfall and its event can be found in the Methods. Data sources of hourly precipitation, rice phenology, rice production are the GPM IMERGv6[22], Jägermeyr et al.[29], and the FAOSTAT[30], respectively. The map was generated in MATLAB R2020a (MATLAB and Statistics Toolbox Release R2020a, The MathWorks). The base map of the country boundaries was from the Global Administrative Areas dataset (https://gadm.org).

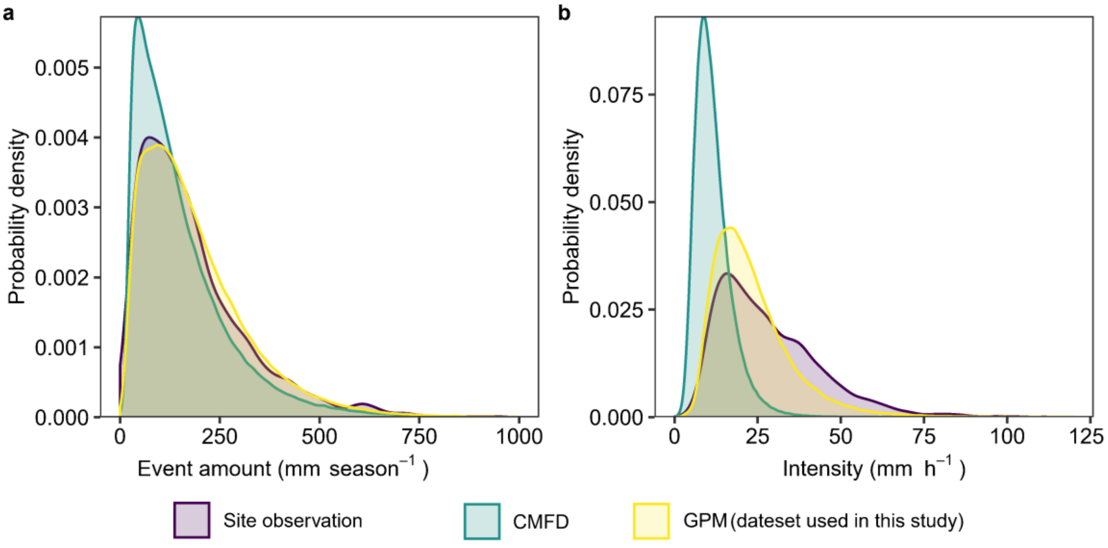

Supplementary Fig. 16 Probability distributions of extreme rainfall from three data sets during 2001-2016. a. Extreme rainfall event amount during rice growing season; **b.** Extreme rainfall intensity during rice growing season. Three data sets include the site observation from the China Meteorological Administration (CMA), the China Meteorological Forcing Dataset (CMFD, http://data.tpdc.ac.cn/en/data/8028b944-daaa-4511-8769-965612652c49/), and global precipitation measurement (GPM) IMERGv6, ref[22].

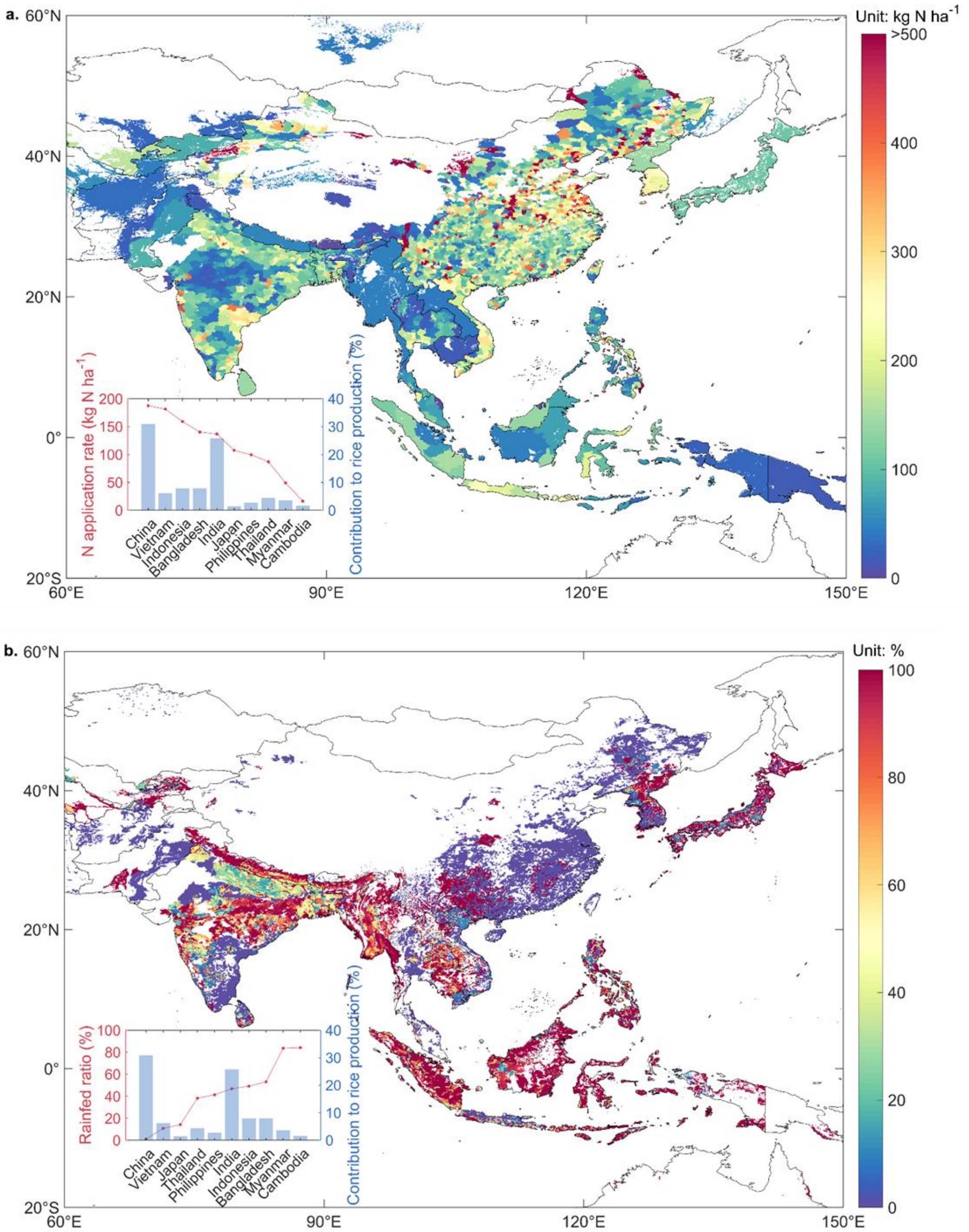

Supplementary Fig. 17 N application rates and rainfed ratios across the Asian rice fields. **a**. N application rate[24], **b**. rainfed ratio[30]. The map was generated in MATLAB R2020a (MATLAB and Statistics Toolbox Release R2020a, The MathWorks). The base map of the country boundaries was from the Global Administrative Areas dataset (https://gadm.org).

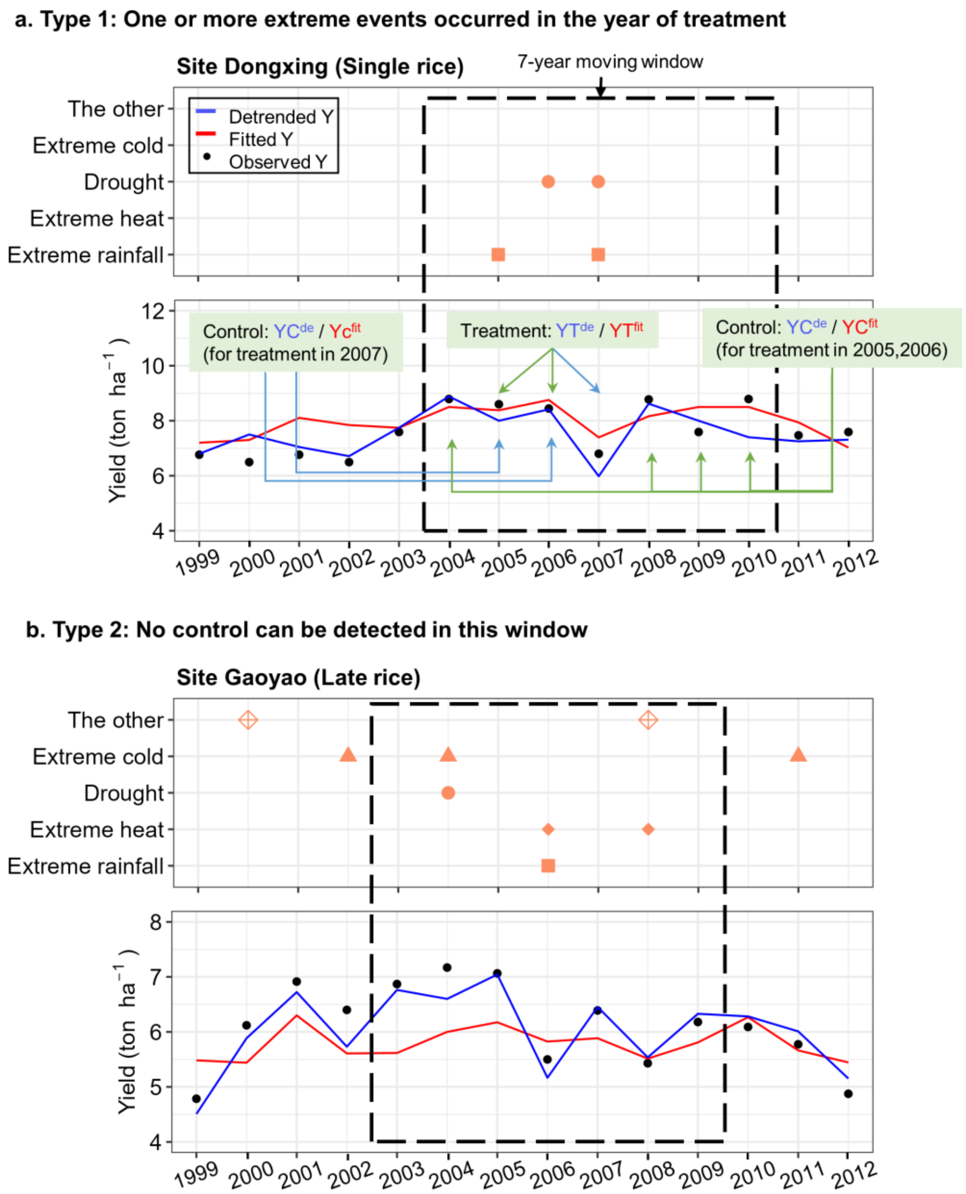

Supplementary Fig. 18 Examples to identify the control-treatment pairs using a window searching strategy. a. Case where one or more extreme climate type in the year of treatment and several corresponding controls. For extreme rainfall event, there are two control-treatment pairs: 1) the year of treatment is 2005, and the years of control include 2004 and 2008-2010; 2) the year of treatment is 2007, and the year of control is 2006. For drought event, there are also two control-treatment pairs: 1) the year of treatment is 2006, and the years of control include 2004 and 2008-2010; 2) the year of treatment is 2007, and the year of control is 2005. **b.** Case in which no control that can be detected in this window and it was not possible to create a control-treatment pair, and thus not involved in the ΔY quantification. Examples are selected from specific sites labeled with site and rice type on the left top of each panel. Points in the top of each panel represent for different extreme events. The blue line in the bottom panels represent the detrended yields, while red lines show the fitted yields and black dots represent the actual rice yields. Black dotted boxes show the 7-year windows, within which all available control-treatment pairs can be identified.

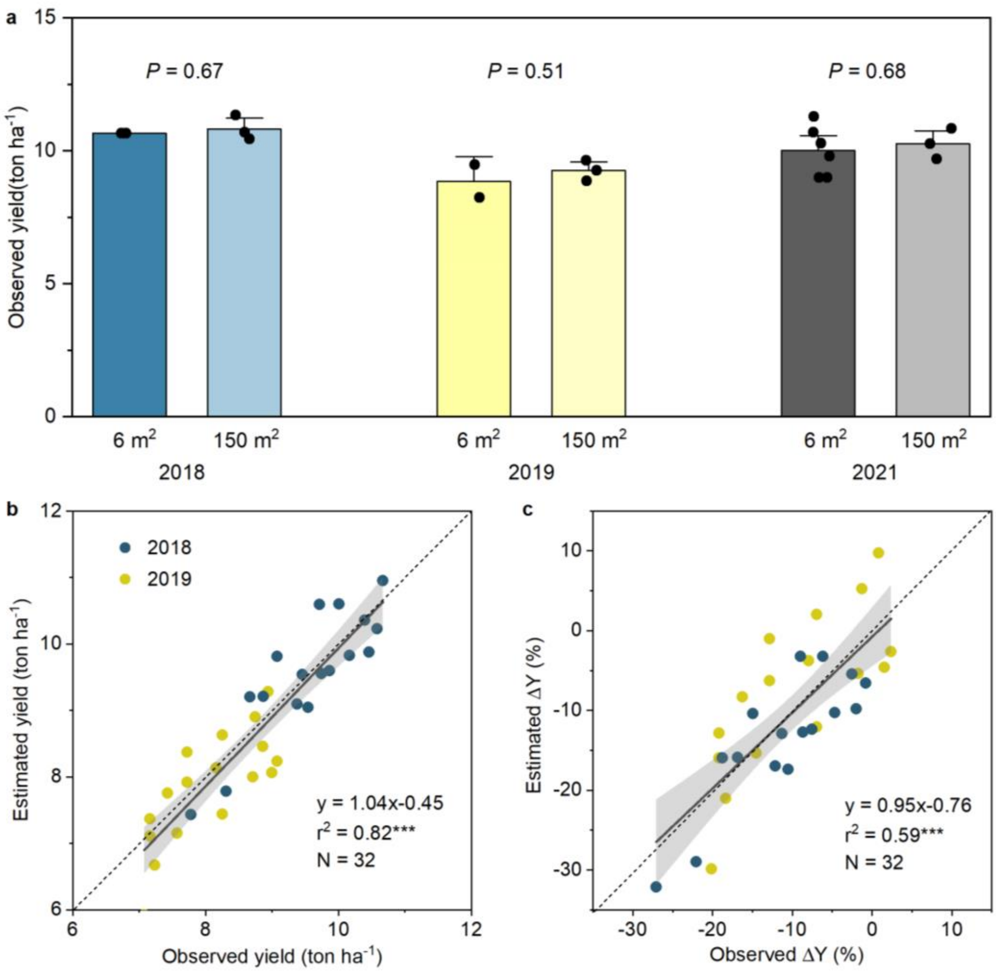

Supplementary Fig. 19 Comparison of yield observations and estimation from yield components. a. Yield observations from adjacent plots owning 6 m^2 and 150 m^2 in 2018, 2019 and 2021 under control, with n = 2 for 2018 and 2019 and n = 6 for 2021 of left columns of each pair, and n = 3 for the right columns of each pair. Data are presented as mean ± standard error. **b**. Observed and estimated yield (n = 16 for each year). **c**. Observed and estimated change in rice yield (ΔY). Column in panel **a** is shown as mean ± standard deviation. The significance between adjacent plots owning 6 m^2 and 150 m^2 were tested using two-sided Paired Samples Wilcoxon Signed Rank Test. The solid line is the best-fit line and shaded area is the 95% confidence interval (estimated from 1,000-time bootstrap analysis), with ***p<0.001.

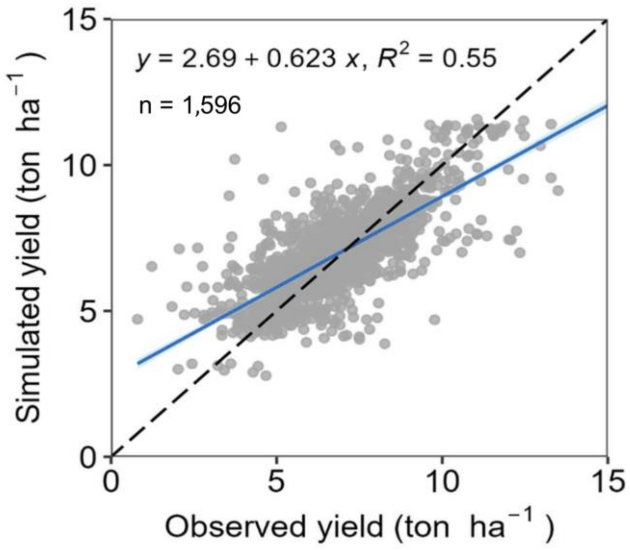

Supplementary Fig. 20 Performance of the panel regression model to exclude the effects from inter-annual variations in climate conditions. The panel regression model was built on all observations where no extreme climate events occurred, with n = 1,596.

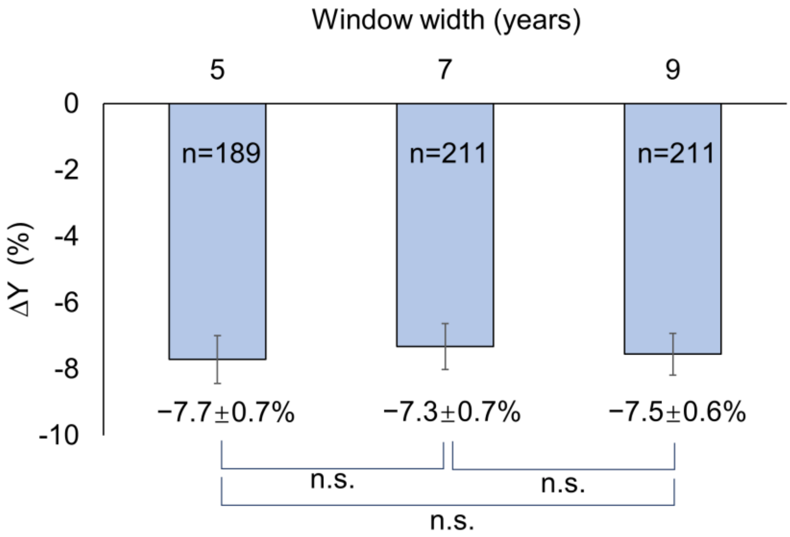

Supplementary Fig. 21 Comparison of ΔY in response to extreme rainfall using three window widths. Data are presented as mean ± standard error. The significance among the three window widths were tested using two-sided Paired Samples Wilcoxon Signed Rank Test with α=0.05.

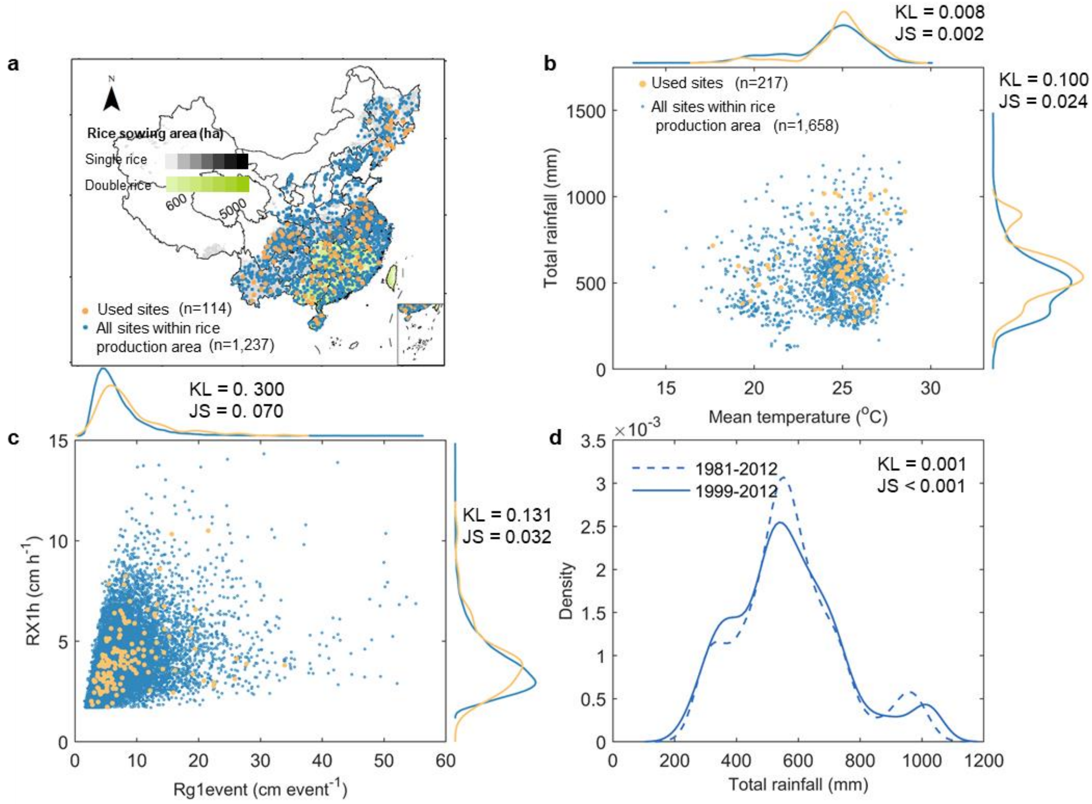

Supplementary Fig. 22 Nationwide observational stations within the rice production areas in China during 1999-2012. a. Spatial patterns of the stations used for all control-treatment pairs and all stations across China's rice production areas. **b**. Distribution of mean temperature and total rainfall during rice growing season and their kernel probability density curves. Each point represents for one station of a year. **c**. Distribution of the extreme rainfall parameters of event amount (Rg1event) and the maximum hourly intensity (RX1h) during rice growing season and their kernel probability density curves. **d**. Kernel probability density curves of total rainfall during rice growing season from study stations in 1999-2012 with that at all stations in 1981-2012. KL and JS represent the Kullback-Leibler divergence and Jensen-Shannon divergence, respectively. The map was generated in MATLAB R2020a (MATLAB and Statistics Toolbox Release R2020a, The MathWorks). The base map of the country boundaries was from the Global Administrative Areas dataset (https://gadm.org).

References:

1 Lesk, C., Rowhani, P. & Ramankutty, N. Influence of extreme weather disasters on global crop production. *Nature* **529**, 84-87, doi:10.1038/nature16467 (2016).

2 Lesk, C., Coffel, E. & Horton, R. Net benefits to US soy and maize yields from intensifying hourly rainfall. *Nat Clim Change* **10**, 819-822, doi:10.1038/s41558-020-0830-0 (2020).

3 Li, Y., Guan, K. Y., Schnitkey, G. D., DeLucia, E. & Peng, B. Excessive rainfall leads to maize yield loss of a comparable magnitude to extreme drought in the United States. *Global Change Biol* **25**, 2325-2337, doi:10.1111/gcb.14628 (2019).

4 Beillouin, D., Schauberger, B., Bastos, A., Ciais, P. & Makowski, D. Impact of extreme weather conditions on European crop production in 2018. *Philos T R Soc B* **375**, 20190510, doi:http://doi.org/10.1098/rstb.2019.0510 (2020).

5 Nath, H. K. & Mandal, R. Heterogeneous Climatic Impacts on Agricultural Production: Evidence from Rice Yield in Assam, India. *Asian J Agric Dev* **15**, 23-42, doi:10.22004/ag.econ.275687 (2018).

6 Shi, W. J., Wang, M. L. & Liu, Y. T. Crop yield and production responses to climate disasters in China. *Sci Total Environ* **750**, 141147, doi:10.1016/j.scitotenv.2020.141147 (2021).

7 Troy, T. J., Kipgen, C. & Pal, I. The impact of climate extremes and irrigation on US crop yields. *Environ Res Lett* **10**, 054013, doi:https://doi.org/10.1088/1748-9326/10/5/054013 (2015).

8 Abbas, S. & Mayo, Z. A. Impact of temperature and rainfall on rice production in Punjab, Pakistan. *Environ Dev Sustain* **23**, 1706-1728, doi:10.1007/s10668-020-00647-8 (2021).

9 Davis, K. F., Chhatre, A., Rao, N. D., Singh, D. & DeFries, R. Sensitivity of grain yields to historical climate variability in India. *Environ Res Lett* **14**, 064013, doi:10.1088/1748-9326/ab22db (2019).

10 Zhu, P. *et al.* The critical benefits of snowpack insulation and snowmelt for winter wheat productivity. *Nat Clim Change* **12**, 485-490, doi:10.1038/s41558-022-01327-3 (2022).

11 Beer, C. *et al.* Terrestrial Gross Carbon Dioxide Uptake: Global Distribution and Covariation with Climate. *Science* **329**, 834-838, doi:10.1126/science.1184984 (2010).

12 van Erven, T. & Harremoes, P. Renyi Divergence and Kullback-Leibler Divergence. *Ieee T Inform Theory* **60**, 3797-3820, doi:10.1109/Tit.2014.2320500 (2014).

13 Comaniciu, D. An algorithm for data-driven bandwidth selection. *Ieee T Pattern Anal* **25**, 281-288, doi:Doi 10.1109/Tpami.2003.1177159 (2003).

14 Liu, J. G. *et al.* A high-resolution assessment on global nitrogen flows in cropland. *P Natl Acad Sci USA* **107**, 8035-8040, doi:10.1073/pnas.0913658107 (2010).

15 Fu, J. *et al.* Nationwide estimates of nitrogen and phosphorus losses via runoff

from rice paddies using data-constrained model simulations. *J Clean Prod* **279**, 123642, doi:10.1016/j.jclepro.2020.123642 (2021).
16 Bulman, P. & Smith, D. L. Post-Heading Nitrogen Uptake, Retranslocation, and Partitioning in Spring Barley. *Crop Sci* **34**, 977-984, doi:10.2135/cropsci1994.0011183X003400040028x (1994).
17 Salles, C., Poesen, J. & Sempere-Torres, D. Kinetic energy of rain and its functional relationship with intensity. *J Hydrol* **257**, 256-270, doi:10.1016/S0022-1694(01)00555-8 (2002).
18 Lu, D., Yang, Y. J. & Fu, Y. F. Interannual variability of summer monsoon convective and stratiform precipitations in East Asia during 1998-2013. *Int J Climatol* **36**, 3507-3520, doi:10.1002/joc.4572 (2016).
19 Nanko, K., Moskalski, S. M. & Torres, R. Rainfall erosivity-intensity relationships for normal rainfall events and a tropical cyclone on the US southeast coast. *J Hydrol* **534**, 440-450, doi:10.1016/j.jhydrol.2016.01.022 (2016).
20 Sitch, S. *et al.* Recent trends and drivers of regional sources and sinks of carbon dioxide. *Biogeosciences* **12**, 653-679, doi:10.5194/bg-12-653-2015 (2015).
21 GML, *Trends in Atmospheric Carbon Dioxide*, U.S. Department of Commerce (2021), Date accessed: 15th October 2021, https://gml.noaa.gov/ccgg/trends/.
22 Huffman, G. J., Stocker, E. F., Bolvin, D. T., Nelkin, E. J. & Tan, J., *GPM IMERG Final Precipitation L3 Half Hourly 0.1 degree x 0.1 degree V06, Greenbelt, MD*, Goddard Earth Sciences Data and Information Services Center (GES DISC) (2019), Date accessed: 5th August 2021, https://disc.gsfc.nasa.gov/datasets/GPM_3IMERGHH_06/summary.
23 Wang, W. L., *A dataset of ten-day values of crop growth and development and farmland soil moisture in China*, National Meteorological Information Center Meteorological Data Office (2019), Date accessed: 4th November 2019, http://data.cma.cn.
24 Zhan, X. Y. *et al.* Improved Estimates of Ammonia Emissions from Global Croplands. *Environ Sci Technol* **55**, 1329-1338, doi:10.1021/acs.est.0c05149 (2021).
25 Yang, H., Jiang, Z. H. & Li, L. Biases and improvements in three dynamical downscaling climate simulations over China. *Clim Dynam* **47**, 3235-3251, doi:10.1007/s00382-016-3023-9 (2016).
26 Moss, R. H. *et al.* The next generation of scenarios for climate change research and assessment. *Nature* **463**, 747-756, doi:10.1038/nature08823 (2010).
27 Vicente-Serrano, S. M., Begueria, S. & Lopez-Moreno, J. I. A Multiscalar Drought Index Sensitive to Global Warming: The Standardized Precipitation Evapotranspiration Index. *J Climate* **23**, 1696-1718, doi:10.1175/2009jcli2909.1 (2010).
28 Wang, S. A. *et al.* Reduced sediment transport in the Yellow River due to anthropogenic changes. *Nat Geosci* **9**, 38-41, doi:10.1038/Ngeo2602 (2016).
29 Jägermeyr, J. *et al.* Climate impacts on global agriculture emerge earlier in new generation of climate and crop models. *Nat Food* **2**, 873-885,

doi:10.1038/s43016-021-00400-y (2021).
30 FAOSTAT, *Crops and livestock products*, Food and Agriculture Organization of the United Nations (FAO) (2019), Date accessed: 20th September 2019, http://www.fao.org/faostat/en/#home.